This dissertation/thesis/report entitled:

written by:

has been approved for the degree of:

in

by

1 - Advisor Name

2 - Department Chair or Committee Member Name

3 - Committee Member Name

4- Committee Member Name

5 - Committee Member Name

6 - Committee Member Name

Month YEAR

Comparative Study of Experimental and Modeled Hydrochar Surface Properties

By:

Max Moran

A Thesis

Submitted to the Faculty

Of the

WORCESTER POLYTECHNIC INSTITUTE

In partial fulfillment of the requirements for the

Degree of Master of Science

In

Chemical Engineering

August 2021

Approved:

Professor Michael Timko, Thesis Advisor

Professor John Bergendahl, Thesis Committee Member

Professor Aaron Deskins, Thesis Committee Member

Abstract

According to the United Nations, approximately 931 million tons of food waste were generated globally in 2019 [1]. This large amount of wastes contributes to various societal and environmental problems, including greenhouse gas emissions and other forms of pollution [2, 3]. One approach to addressing negative impacts of food waste is water valorization, a process of converting waste materials into more useful products, such as useful chemicals and materials. Hydrothermal carbonization (HTC) is a valorization process, where wet biomass is converted through a chemical process under elevated temperatures and pressures into a solid hydrothermal char. These chars can be used for a variety of applications, including water purification, gas storage, and soil amendments. One challenge with developing chars for certain applications is that the structure of chars, especially more complex chars from nitrogen bearing waste streams, is not well defined. In this research study, various hydrochars was investigated through different experimental methods in order to develop an understanding of structural properties. The two main methods for gaining structural insight were NMR spectroscopy and Boehm titration. A model structure was created from NMR data by collaborators at Brandeis University and was compared to previous proposed structures from literature. Boehm titrations were carried out in order to gain further experimental insight into the structure/surface properties of the char. The data from these methods were compared to examine whether the methods resulted in agreement on surface site properties. The NMR and titration surface data were also used with a mathematical model to see whether the macroscopic properties of a char, e.g. zeta potential, can be predicted from surface data. The results showed that the NMR and titration data agreed, further validating the proposed NMR model. Also, both the NMR and Boehm titration data were able to create model data fits to certain experimental zeta potential curve characteristics.

Acknowledgements

I want to thank my advisor, Professor Timko, for the advice and help that he provided throughout my project. I also want to thank Professor Bergendahl and Professor Deskins for serving as part of my thesis committee. I greatly appreciate the efforts of Professor Klaus Schmidt-Rohr and his team at Brandeis in providing the NMR work and analysis for the hydrochars. I want to thank Professor Bergendahl and Professor Deskins for serving as part of my thesis committee. I want to thank Geoff Tompsett for helping to run surface area experiments on the hydrochars and for all other advice and help he provided over this project. I want to thank Louise Delahaye for providing procedures for synthesis and analysis, as well as answering many questions regarding throughout the project providing assistance. I also want to thank Eugena Choi for assisting in synthesizing some hydrochar samples. I want to thank Ziyang Zhang for his advice on zeta potential measurements and analysis. I would also like to thank Ayten Ates for providing her procedure in running zeta potential measurements on hydrochars. Finally, I would like to thank my parents for the support and assistance throughout the work on my project.

Table of Contents

Table of Figures

Table of Tables

Introduction

According to the United Nations, 931 million tons of food waste were generated in 2019 [1]. This includes food that never leaves farms, gets spoiled in the supply chain, or thrown out in homes, restaurants, etc. [2].

	Global average food waste (kg/capita/year)*	2019 total (million tonnes)
Household	74	569
Food service	32	244
Retail	15	118
Total	121	931

Figure 1: *Table of food waste estimates from United Nations report [1]*

This massive amount of food waste is not only a waste of food that can be used to feed the global undernourished, but it also creates significant impacts on the environment as well. The energy and resources that went into growing and transporting food is wasted and if the food is landfilled it can increase greenhouse gas emissions. Eliminating food waste could reduce the amount of human-generated greenhouse gases by 8%, according to the World Wildlife Foundation [2].

In order to address the issue of food waste, researchers have been examining various opportunities to use food waste as a feedstock in processes. Food waste valorization offers the opportunity to take the waste resources and nutrients in food waste and convert them into useful and sustainable materials. One nutrient present in food waste that is especially problematic is nitrogen. Nitrogen fixation in soil is a very energy intensive process, which accounts for ~1% of

global energy use [3]. Also, fertilizers are often liberally applied to crops resulting in a large amount of nitrogen runoff, which can lead to other environmental issues. Nitrogen-containing carbon materials can be good for certain applications, such as soil amendments to reduce fertilizer use [4, 5], adsorbents for water purification [6], among other possible uses.

This project focused on the waste valorization process of hydrothermal carbonization. This process takes a wet feedstock and creates a carbonaceous solid material. This process takes place under high temperatures (180-280˚C) and pressures (2-6 MPa) in the presence of water, where the organic feed undergoes a chemical reaction to create a porous, polymeric carbon rich char. This material can include nitrogen and other elements as well depending on the feedstock. These hydrothermal chars can have a variety of applications including soil amendments, gas storage materials, electrochemically active materials, and water purification sorbents. A challenge in utilizing these chars for certain applications is the lack of detailed structure data, especially for nitrogen-containing chars (N-hydrochars) [7, 8]. This lack of knowledge prevents the ability to rationally design chars for a desired applications.

In this project, the structure of hydrochars were investigated through various methods. Establishing knowledge about the underlying structure of hydrochars is important to understand in what application chars be effectively utilized. This analysis includes extensive structure and modeling analysis and more experimental lab procedures in order to develop an understanding through different levels and accessibilities of experiments. The structure data was also evaluated in its ability to predict macroscopic properties; this can assist in understanding how a char may interact and what applications it may excel in.

Background

Sustainable carbon materials

As the world continues to grapple with the increasing effects of climate change and environmental pollution, researchers are increasingly interested in producing useful sustainable carbon materials. The sustainable materials need to be "low cost, scalable, industrially and economically attractive, and based on renewable and highly abundant resources, whilst of course achieving application performances […] that exceed existing technologies" [9]. Currently, carbon materials are used in a variety of applications: renewable energy technologies, water purification, soil amendments, gas storage, among many other applications [9]. Another benefit of developing sustainable carbon materials is the ability to use waste as a feedstock. Human-created wastes, such as food waste, present a global challenge.

The valorization of food waste, among other wastes, into useful products can be used to address the issues related to food waste and create a feedstock source to create more sustainable carbon materials.

Hydrothermal Carbonization

Hydrothermal carbonization (HTC) is a possible method for the production of sustainable carbon materials. The HTC process takes a wet biomass feed and produces a solid hydrochar, along with liquid and gaseous products. HTC is performed in a temperature range of 180-260˚C [10] and under autogenous pressure (2-6 MPa [10]). Water is one of the central parts of the HTC process, which means that wet biomass feeds can be used without energy-intensive drying beforehand. The main parameter that affects the end product of hydrothermal carbonization is the

process temperature [10].The main desired product from HTC is the solid phase (hydrochar); the side products of the HTC process are gases and a liquid phase (water and bio-oil) [10].

Hydrochar applications

Hydrochar has a wide variety of applications and could be used in the place of similar carbonaceous materials. One possible use is as a renewable coal energy source. There are a few plants worldwide that are currently convert biomass or other waste materials (sewage sludge) into biocoal for energy production through HTC, such as the Terranova Ultra plant in Jinjing, China that can process up to 14,000 tons of sewage sludge per year [11] or the AVA HTC plant in Relzow, Germany [12].

Hydrochar has also been investigated as a possible activated carbon adsorbents for removing water pollutants [13]. In order to have a good adsorption capacity, hydrochar often needs to be activated using a base solution. The base solution “activates” the functional groups on the surface of the hydrochar which increase the adsorption capacity significantly [13]. Hydrochars have been compared to similar biochar products from pyrolysis for heavy metal sorption. In these studies, they were found to outperform the pyrolysis biochars, making them a more attractive material for water purification [14, 15, 16].

Hydrochar is also being investigated for its potential use in agriculture. Hydrochar presents the potential to be used as a soil amendment to assist in the growing of crops and helping the health of the soil. One of the real world example that indicates the possibility of hydrochars usefulness in soil is the Terra Preta soils in the Amazon; these soils contain high nutrient levels and high levels on charcoal that adsorbed nutrients and prevented them from leaching in the soil [5]. This presents an analogous natural example of a carbonaceous material

improving the health of the soil. The possibility of hydrochars to provide similar useful properties to soil has generated much research interest. In the case of hydrochars, it is expected that specifically nitrogen-containing chars (N-hydrochars) may be a good fit for soil amendments. Studies of hydrochar as soil amendments have found that "hydrochar is an environmentally friendly soil amendments for plant growth by slow release of nutrients and carbon sequestration" [36]. However, the applicability and properties of hydrochar for certain desired soil effects depends on starting conditions and feeds for the materials.

Char Structure

One of the challenges in identifying appropriate uses for hydrothermal chars is the understanding of the underlying structure. The structure of the char is dependent on a number of factors, including reaction time, reaction temperature, pH, and feedstock. In designing a char for a specific application, knowledge of the molecular structure would provide information to make scientific decisions in the production of the char rather than relying on solely empirical data. For example, when designing a nitrogen containing hydrochar, the location of the nitrogen within the molecular structure could help determine the hydrochar's usefulness for certain applications. If the nitrogen is present in bio-available groups, then it could be appropriate for a soil amendment [5]; if the nitrogen was present in a thermally-stable group, then it would be better suited for an adsorbent or for upgrading into an activated carbon [17]. The lack of understanding of the molecular structure presents a roadblock in the rational design of chars for desired applications.

Various hydrochar structure models have been proposed in the literature, such as arene rich structures based on Raman spectroscopy data and furan-arene linked structures based on NMR data, shown as (a) and (b) respectively in figure 2.

(a) (b)

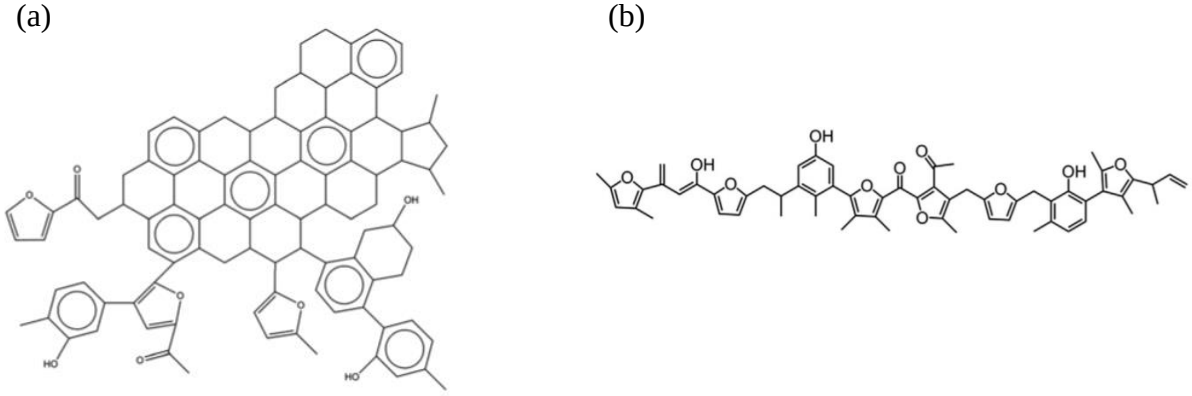

Figure 2: *Hydrochar literature structure models (a) Chutanapum et al. [19] (b) Latham et al. [20]*

However, an issue was discovered in the Raman analysis of hydrochars; in Raman spectroscopy, the hydrochar was broken down by laser irradiation causing thermal artifacts [20]. This results in the furans within the chemical structure to transition to arene groups [20]. This discrepancy along with reaction pathway analysis that indicates the structure should be composed of furans [20] indicated that the NMR based structure was likely closer to the true structure of hydrochar.

In collaboration with Brandeis University and Prof. Klaus Schmidt-Rohr, we have studied the structure of hydrochars using NMR. Brandeis simulated previous predicted structures and compared them with the experimental NMR of a glucose hydrochar. The analysis is shown below in figure 3.

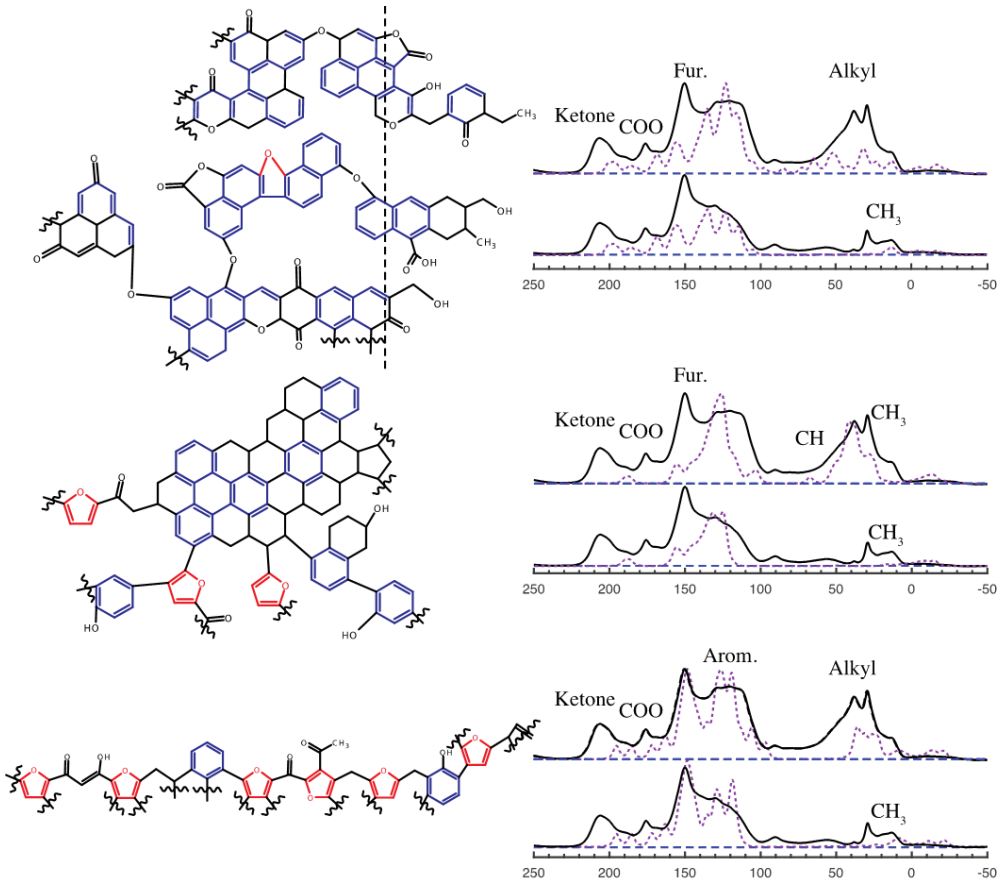

Figure 3: *NMR analysis of literature structures and simulated spectrum comparison to experimental spectrum, carried out by Prof. Schmidt-Rohr et al., Brandeis University*

In their simulation experiments, none of the evaluated predicted models, presented a good fit for the experimental NMR spectrum. This illustrated the need for a better structural model to better represent the actual observed structural characteristics in the NMR results. Using NMR fitting and pattern recognition techniques, Brandeis developed a predicted molecular structure for a basic glucose hydrochar that would fit the experimental NMR data. The structure, as seen below in figure 4, is a mixed-model of furan and arene ring structures.

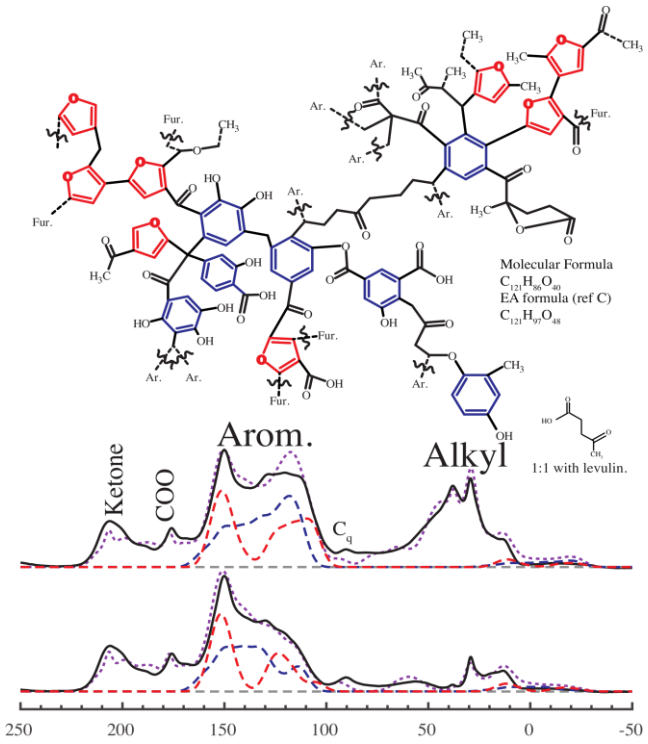

Figure 4: *New NMR glucose hydrochar mixed-model structure and spectrum comparison, carried out by Prof. Schmidt-Rohr et al., Brandeis University*

The fit of this structures simulated spectrum with the experimental spectrum was better than that of the literature structures that were analyzed. This structure is expected to be a better overall representation for the actual molecular structure than the presented literature structures. This structure will be analyzed and evaluated along with the literature structures for the ability to predict or reflect macroscopic properties of hydrochar. This comparison will allow for validation or indicate discrepancies for the new model structure.

Char Properties

The two main macroscopic properties of hydrochar that are the focus of this paper are acid/base surface sites and zeta potential. These properties are measurable or calculable

properties of hydrochar as well as being important factors in possible applications of char and indicators for the behavior of the char.

Surface Sites

Oxygen-containing functional groups (OFGs) are an important characteristic of a hydrochar. A high number of OFGs can indicate an effective precursor for chemically activated carbons. These sites are especially important for adsorption based applications. It has been found that oxygen functional groups play an important role in binding and retaining heavy metals in both water adsorption studies [13] and soil studies [21].

The quantification of these sites is often carried out by a method called Boehm titration [22]. This method is often used for carbons, especially activated carbon materials. It involves mixing a carbon material with a certain amount of base/acid and then quantifying how many acid sites are present based on how much of the reaction base or acid is left after removal of the carbon.

Because the various steps in the Boehm titration method can be carried out in different ways, a lack of standardization makes it difficult to compare the method's results across different experiments and research groups. The Boehm method has been used for quantification of surface on hydrochars previously [24, 25], but it is difficult to verify results due to the empirical nature of the method. From the hypothesized molecular structure from NMR, the number and density of acid sites can be estimated. An analysis of this data and the Boehm titration results can assist in assessing the results of both approaches. If the results correlate and are similar, we can develop more confidence in the NMR structure and its ability to predict macroscopic properties, while also gaining some confidence in the Boehm titration. If both methods are able to produce similar

data, it would give confidence in analyses of different complexities to provide useful insights into char structures.

Zeta Potential

The strongest sorbate-hydrochar interaction has been found to be electrostatic [13, 25]. This is due to the dissociation of the functional groups on the surface of the char giving the particle a negative charge. The negatively charged particle can then interact with positively charged cations and adsorb materials such as heavy metal ions.

The dissociation of surface sites give the particle a charge and lead to the phenomena called the electrical double layer (EDL) [25]. The main sections of the EDL are the Stern layer and the diffuse layer. The Stern layer is the layer of opposite charged ions, compared to the char surface, which is fixed to the particle. The diffuse layer is the layer outside of the Stern layer, where ions of varying charges are loosely associated with the particle. The solution medium outside of these layers is the bulk solution. [25]

An important electrostatic characteristic within the EDL is the zeta potential. The zeta potential is the potential difference between the bulk solution and the fluid associated with the particle [26]. A diagram of the electrical double layer and zeta potential can be seen below in figure 5. This boundary between the diffuse layer and bulk solution is known as the slipping plane.

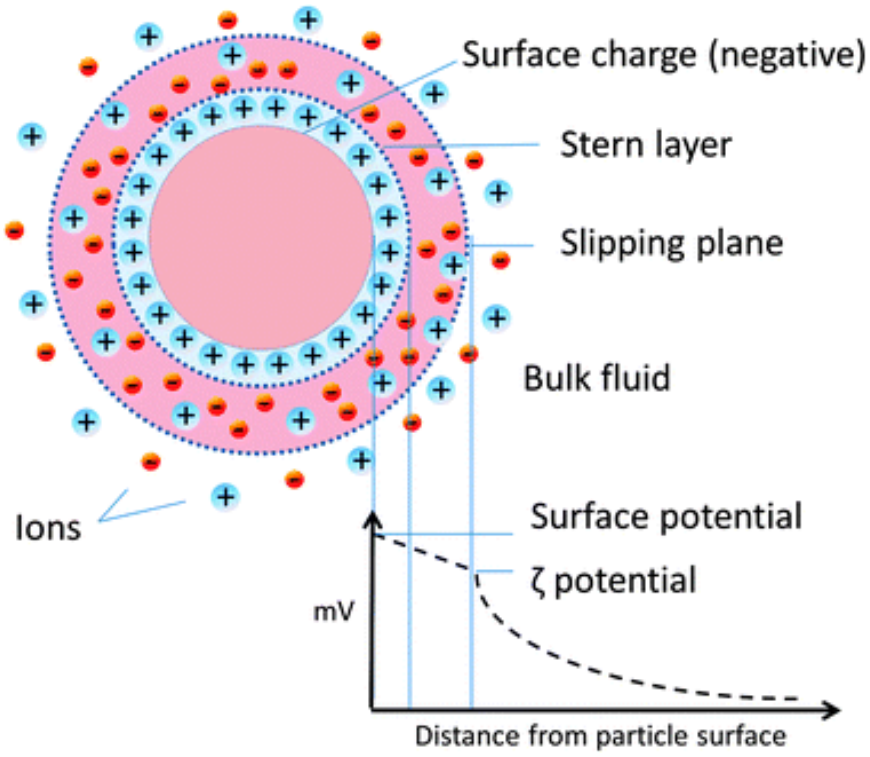

Figure 5: *Diagram of electrical double layer with locations of different potential values*

One issue with the determination of the zeta potential is that the slipping plane is not a well-defined boundary, because the diffuse layer can move under stress among other particle conditions [28]. The location of the slipping plane can be dependent on the particle and what is adsorbed to the surface [28]. Because the main mechanism for cation sorption in hydrochars is electrostatic, the zeta potential is an important characterization for chars. High absolute zeta potentials indicate high absolute surface charges on particle. This increased surface charge can help promote electrostatic interactions, which can promote adsorption.

An important element of zeta potential measurements is the point zero charge (PZC). This is the pH point at which the surface charge on the particle is neutral (=0). This point is important for understanding ideal adsorption conditions. If the solution's pH is above the PZC, the particle would be negatively charged, which would be ideal conditions for adsorbing cations.

If the solution's pH is below the PZC, the particle would be positively charged, which would be ideal for adsorbing anions. This characteristic can be estimated from zeta potential graphs and is an important factor when understanding how to best use a char for certain applications.

The zeta potential of particles can be calculated from measurable experimental properties (e.g. electrophoretic mobility) [28]. The zeta potential can also be calculated through equations relating surface potential and surface charge density of the particle. These equations are an important part of this study because they are used to calculate the predicted zeta potential from the NMR and titration data. The ability to predict properties from surface data would help to provide insight on different hydrochars and their functionality for certain applications, such as adsorbents. The equations used for the zeta potential model in this paper are presented below.

Surface Charge Density Equation #1:

There are two surface charge density equations. The first is:

$$\sigma_0 = \frac{\varepsilon_0 \varepsilon_3 \kappa k_b T}{2\pi e}\left[\sinh\left(\frac{e\psi_0}{2k_b T}\right) + \frac{2}{\kappa a}\tanh\left(\frac{e\psi_0}{4k_b T}\right)\right]$$

This equation is mostly constant values, assuming the solution medium is water at room temperature. The two varying values in this equation are ψ_0 andκ. The symbols are defined below:

ε_0: Dielectric constant of vacuum

ε_3: Dielectric constant of water

κ: Inverse Debye length.

k_b: Boltzmann constant

T: Temperature (K)

e: Electron unit charge

ψ_0: Surface potential (V)

a: radius of your particles

The inverse Debye length is defined as:

$$\kappa = \lambda_D^{-1} = \sqrt{\frac{\sum(z_i e)^2 c}{\varepsilon_0 \varepsilon_3 k_b T}}$$

The undefined symbols in this equation are:

z: Valance. In 1:1 electrolyte, z=1.

c: Ion concentration (add units)

Surface Charge Density Equation #2:

The second surface charge density equation is:

$$\sigma_0 = eN_A \{-\Gamma_{A^-} - \Gamma_{B^-} + \Gamma_{C^+} + \cdots\}$$

The symbols in this equation are:

N_A: Avogadro's number (6.022*10^23)

$\Gamma_{A^-}, \Gamma_{B^-}, \Gamma_{C^+}$: Group surface coverage that dissociates

The surface groups that dissociate is a function of a few equations. These equations can be rearranged in order to solve for the $\Gamma_{i^{-/+}}$ groups for the surface charge density equations:

$$k_{a_1} = \frac{[H^+]_0 \Gamma_{A^-}}{\Gamma_{AH}}$$

$$\Gamma_{A_t} = \Gamma_{AH} + \Gamma_{A^-}$$

$$[H^+]_0 = [H^+]_b \, exp(-\frac{e\psi_0}{k_b T})$$

$$[H^+]_b = 10^{-pH}$$

The symbols in this equation include:

Γ_{A_t}: Total group surface coverage

Γ_{AH}: Group surface coverage that does not dissociate

pH: Bulk phase pH

k_{a_1}: Acid dissociate constant

Surface Potential Equation:

Once the values for total group surface coverage are known, as well as the concentration and pH conditions of the solution, the two surface charge density equations can be set equal to each other in order to solve for the surface potential, ψ_0. The surface potential value can be used to solve for the zeta potential through the equation:

$$\psi_0 = \frac{4k_bT}{ze}\tanh^{-1}(\tanh(\frac{ze\zeta}{4k_bT}) \times e^{\kappa d})$$

The new variables in this equation are:

ζ: Zeta potential (V)

d: Distance between particle surface and slipping plane, often taking the value of 5-6 Å

Methodology

Hydrothermal Char Synthesis

As part of this project, multiple different hydrochars were developed to explore the effect of starting materials on the characteristics of the chars. Three types of chars were examined: a model glucose char, chars with additional acidic starting components, and chars with nitrogen containing starting components. The chars and process to synthesize them are summarized below.

Glucose-HCl Hydrochar

First a glucose char was synthesized for a base model char. This char consisted of a 20 wt% glucose solution with deionized (DI) water and 0.16M Hydrochloric Acid (HCl). Around 20 g of glucose was mixed with 80g of DI water and 3 mL of 5M HCl. After mixing the solution for 30 minutes, the solution was placed in a Teflon reactor inlet, which was then placed into a steel autoclave. The autoclave was placed in an oven at 180 °C for 16 hours. After 16 hours, the oven was shut off and the autoclave allowed to cool for around 12 hours.

Figure 6: *Steel autoclave where Teflon inlet was placed for heating in oven*

After cooling down, the Teflon inlet was removed and the resulting hydrochar and aqueous mixture was mixed with 200mL of a 50:50 ethanol and water solution. After mixing for 15-30 minutes, the solution was vacuum filtered with a Buchner funnel to separate the solid product from the liquid.

Figure 7: *Vacuum filtration setup for separating solid from aqueous phase*

The washing and filtering steps were repeated three times. The washed hydrochar was then dried in an oven at 65 °C for at least 12 hours. After drying, the char was ground into a powder and placed in vial.

Figure 8: *Glucose hydrochar after 65 °C drying*

Acrylic Acid

Acrylic acid chars were synthesized to examine the effect of additional initial acid content on the structure and properties of the char. Two different chars were made: one with 10% glucose, 5% acrylic acid, 85% DI water and one with 10% glucose, 10% acrylic acid, 80% water. Both followed the same procedure. First, the acrylic acid, DI water, and glucose were mixed for 30 min. The mixture was then placed in a Teflon inlet, in a steel autoclave, which went into an oven at 190°C for 16 hours. The oven was shut off and the autoclave was allowed to cool for 12 hours.

The resulting slurry was then washed with water and ethanol and filtered with vacuum filtration, similar to the glucose-HCl procedure. The washed char was then dried at 65°C for at least 12 hours. After drying, the char was ground into a powder and placed in vial.

(a) (b)

Figure 9: *Acrylic acid chars (a) 5% acrylic acid char after filtration (b) 10% acrylic acid char after filtration and drying*

Glucose-Urea Hydrochar Synthesis

Glucose-Urea char was created in order to observe the effect of the addition of nitrogen groups into the hydrochar. A solution of 20 wt% glucose, 0.5M urea, and DI water was made. The pH of the solution was adjusted to around 4 using HCl. The solution was then placed in the Teflon inlet and put in the autoclave. The autoclave was put in the oven at 180°C for 16 hours. After the 16 hours, the autoclave was allowed to cool, and then the aqueous-hydrochar mixture was washed and filtered 4 times with a 50/50 ethanol and water solution. The samples were then dried in the oven for 24 hours and then grinded into a powder.

Figure 10: *Urea char after drying and grinding*

Glycine-Glucose Char

A glycine-glucose char was synthesized in order to observe the effect of adding nitrogen. Glycine is present in many human generated wastes, so incorporating it into chars can provide insight into studying the nitrogen chemistry before using more chemically complex waste feeds for chars. The glycine-glucose char was prepared with a 2:1 mol ratio of glucose to glycine. Both followed a similar procedure. First the appropriate amount of glucose, glycine, and DI water were mixed for around 30 minutes. The solution was then placed in the Teflon inlet and the inlet placed into the steel autoclave. The autoclave was then heated for 16 hours at 180 °C. After cooling, the resulting hydrochar and aqueous slurry was washed with a 50/50 ethanol and water mixture and filtered with vacuum filtration. The solid char product was dried at 65°C for 12 hours and then ground into a powder and stored in a vial.

Figure 11: *Glycine char in vial after drying and grinding*

Surface Area Measurements

Surface area measurements of the hydrochar were measured with nitrogen and carbon dioxide physisorption. The N_2 samples were run at 77 K and the CO_2 samples were run at 273 K. The surface area was determined using the Brunauer-Emmett-Teller (BET) model.

Boehm Titration

Boehm titration was run on all the prepared chars in order to determine the oxygen functional group density on the surface of the chars. Boehm titration uses bases of different strengths in order to determine the number of varying acid sites. Sodium Hydroxide (NaOH) reacts with all the carboxylic, lactonic, and phenolic groups (most acid groups), Sodium Carbonate (Na2CO3) reacts with the carboxylic and lactonic groups (stronger acid groups), and Sodium Bicarbonate (NaHCO3) reacts with just the carboxylic acid groups (strongest acid groups). First, 0.2 g of the hydrochar was placed into a tube and 20 mL of 0.1 M reaction base was added. The tubes were then put on the arm of a shaker where they were shook for 48 hours. After, the sample was vacuum filtered to separate the hydrochar and base solution.

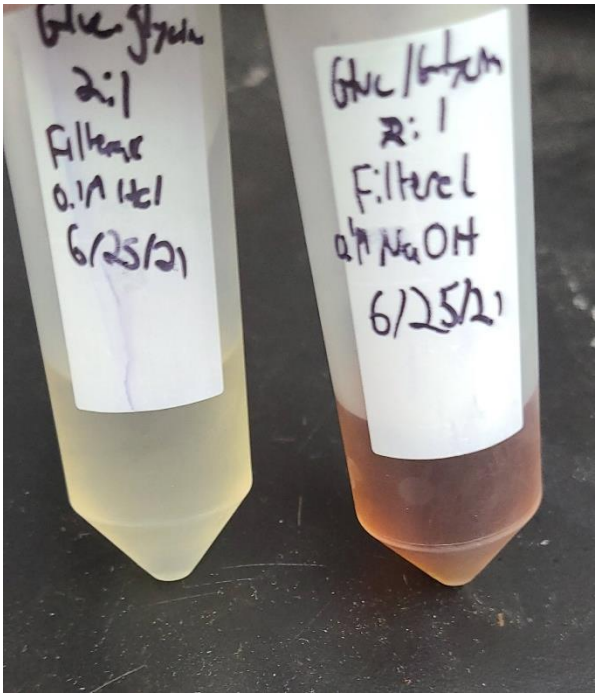

Figure 12: *Filtered solutions of HCl (left) and NaOH (right) after 48 hours of shaking with glycine char*

The base solution was separated into different 5 mL aliquots. To these aliquots, 5mL of water and 5 mL of 0.1 M HCl were added to neutralize the base. The solution was degassed with nitrogen for 1 hour to remove any carbon dioxide. The degassed solution pH was measured and then the solution was titrated with 0.1 M NaOH, until reaching a pH of 7. The equation used to determine the number of carbon surface functionalities (n_{CSF}) is presented below: [22]

$$n_{CSF} = \frac{n_{HCl}}{n_B}[B]V_B - ([HCl]V_{HCl} - [NaOH]V_{NaOH})\frac{V_B}{V_a}$$

Where $\frac{n_{HCl}}{n_B}$ is the molar ratio of acid to base (used for monoprotic vs diprotic bases), [B] and V_B are the concentration and volume of reaction base, [HCl] and V_{HCl} are the concentration and volume of acid added to the aliquot, [NaOH] and V_{NaOH} are the concentration and volume of the

titrant, and V_a is the volume of the aliquot. The density of acid sites was calculated by dividing nCSF by the amount of solid sample added to the reaction base.

A similar procedure was carried out to determine the number of base sites present on the char. However, this was done using direct titration instead of a back titration. ~0.2g of char was mixed with 20 mL of 0.1M HCl. After shaking for 48 hours, the solution was vacuum filtered. A 5 mL aliquot of the HCl solution was placed in a separate tube and degassed with nitrogen for an hour. After degassing, the sample was directly titrated with 0.1M NaOH to a pH of 7 to determine the density of base sites. The equation to calculate n_{CSF} for the direct titration is:

$$n_{CSF} = [A]V_A - [NaOH]V_{NaOH}\frac{V_A}{V_a}$$

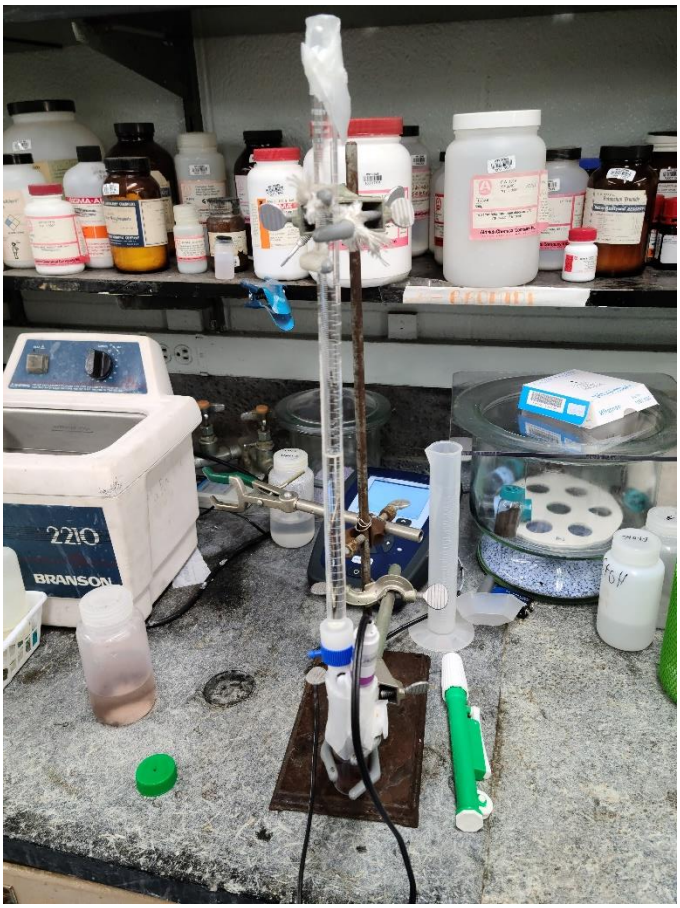

Figure 13: *Boehm titration experimental setup*

Zeta Potential

Zeta potential was measured using a zeta meter (Malvern Zetasizer-Nano-Z). The sample was prepared by adding around 0.01g of the char to a 0.1 N NaCl solution. The char was suspended and homogenized using an ultrasonic bath for 2 hours. After homogenization, the suspension was separated and equilibrated at varying pH values. The equilibrated samples were put into a zeta cell and the zeta potential was determined from the average of three measurements. The point zero charge was estimated from the graph of zeta potential for each char.

Zeta Potential Model

A zeta potential model was created using MatLab software in order to compare the expected zeta potential from the number of acid and base groups as determined by NMR (and titration). The MatLab model was created using the equations presented in the zeta potential background section. The model was run with no modifications in order to examine the curve fit with conservative estimates for initial values. If necessary, reasonable modifications to parameters in equations were used to create a better fit. A sample of the MatLab code can be found in the Appendix B.

Results/Discussion

Acid Sites

Our initial hypothesis was that the NMR mixed-model created by Brandeis is the best predicted molecular structure out of the presented literature structures for hydrochar, since it is consistent with the experimental NMR spectrum.

Hydrochar was added to base solutions to determine the experimental acid and base site densities of the glucose hydrochar. These values were compared to the literature value structures. The literature values for the models in figure 14 were determined by the number of relevant oxygen-functional acid sites (carboxylic, lactonic, phenolic) present in the molecular structure. This was divided by the expected molecular weight of the structure in order to determine the expected acid site density of the model.

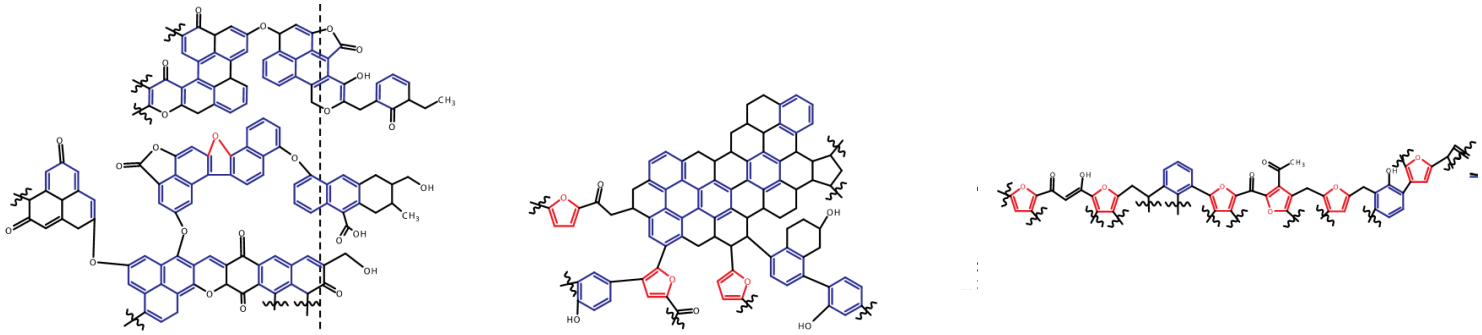

Figure 14: *Literature structure models that were evaluated by NMR analysis*

As seen in figure 15, the literature models do not represent all of the different acid groups detected in the Boehm Titration. The NMR structure model has a total acid site density within the experimental error of the titration of the char. This indicates that it is the best model prediction out of the four presented, as was initially hypothesized.

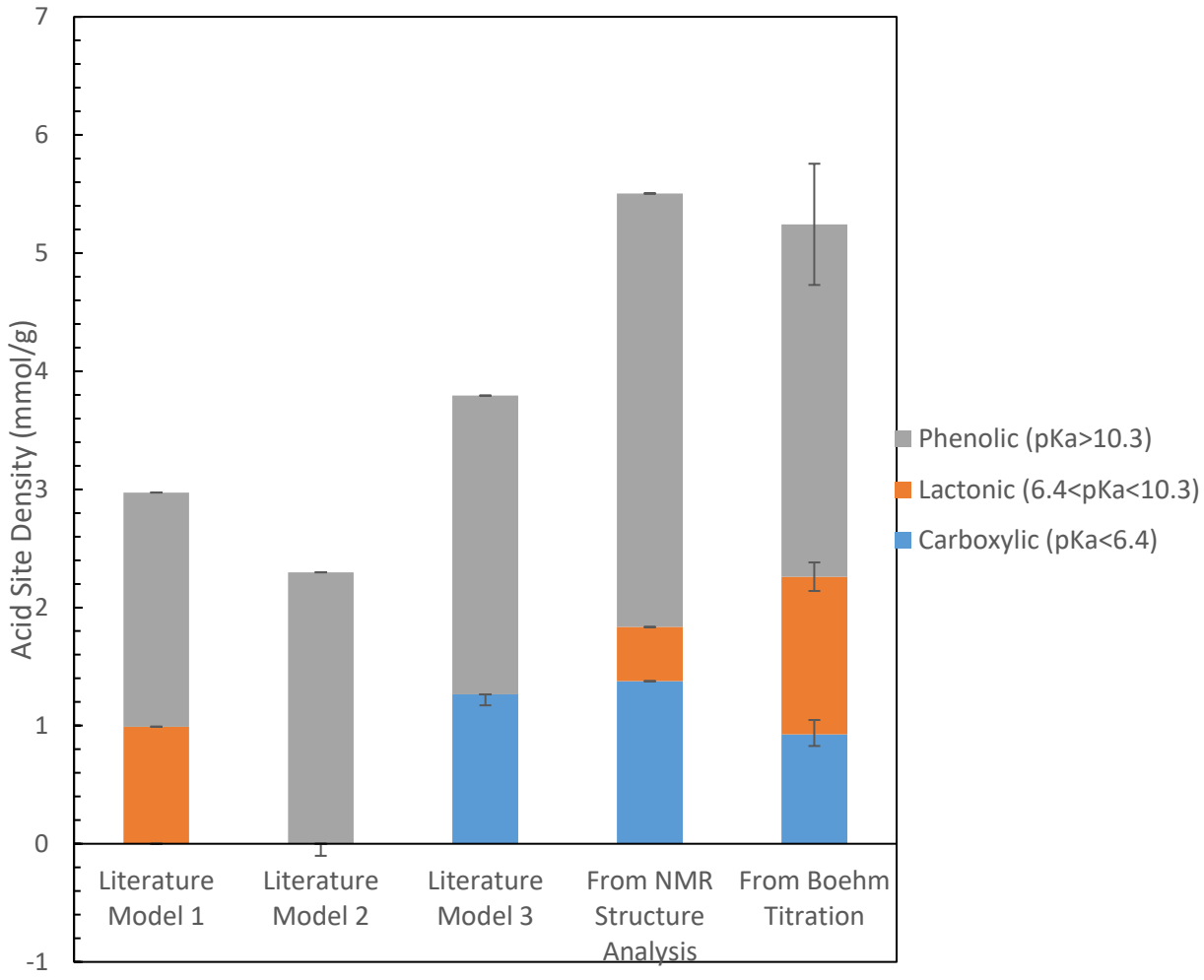

Figure 15: *Acid group breakdown of literature structures and Boehm titration results for glucose hydrochar*

The main difference between the NMR structure acid sites and Boehm determined acid sites is the group breakdown. With the Boehm titration, more lactonic groups and less carboxylic and phenolic groups, were detected than were present in the NMR.

With agreement of the Boehm titration and NMR for the glucose char, the other synthesized chars were titrated to gain insight into the functional groups from the modified conditions and materials. The acid site densities of the chars are present below in figure 16.

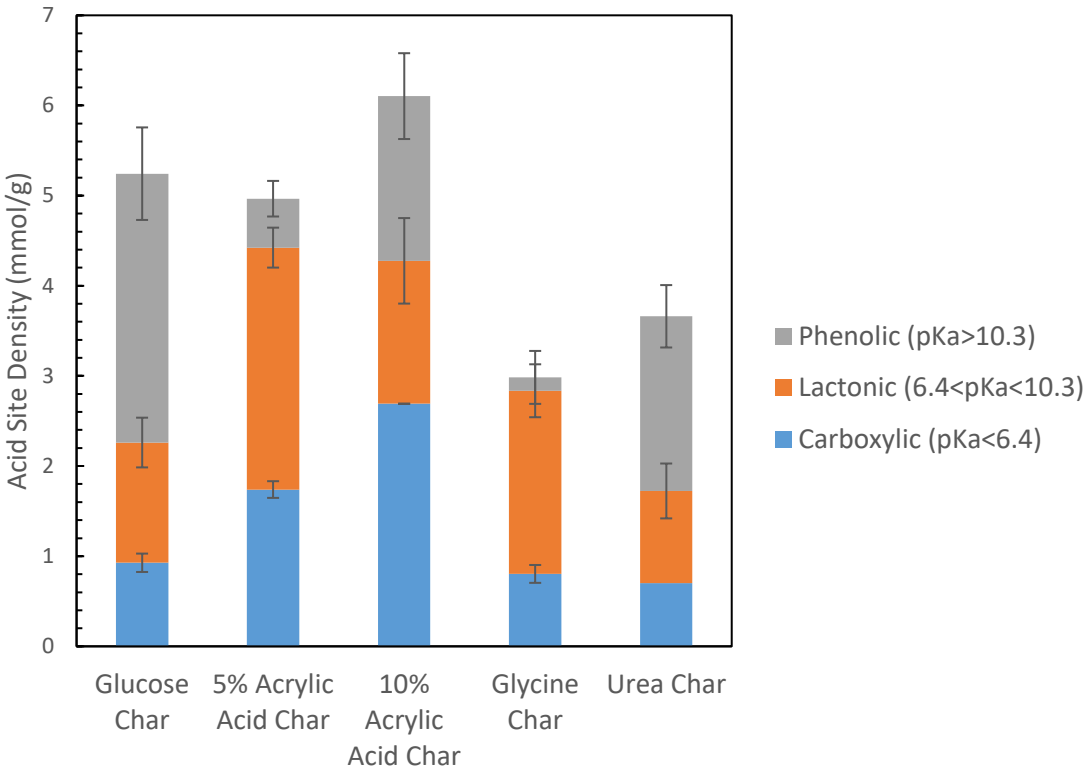

Figure 16: *Boehm titration results for glucose and modified hydrochars acid sites*

The total acid sites of the acrylic acid chars are similar to that of the glucose char. The main trend in the differences in these chars is the detected amount of the strongest acid sites (most likely all carboxylic groups). The glucose char has the least amount of carboxylic sites and adding acrylic acid as starting material increases the amount present of carboxylic sites in the char. This could be beneficial for an adsorption application, due to the importance of carboxylic and carboxylate groups in adsorption [13]. The strong carboxylic acid group density in both the glycine and urea char is comparable to density present in the glucose char. However, the chars with nitrogen containing components, urea and glycine, see a decrease in total acid site density compared to the glucose char. This may reduce the adsorption ability of the chars, but further study with this data is needed. Even with the decrease in acid sites, the doping of nitrogen

containing compounds into hydrochar could benefit a soil amendment applications to increase nutrient and water retention, if the nitrogen is in bioavailable functional groups, [5] as well as N-doped activated carbons, if the nitrogen is in thermally stable groups [29].

With knowledge of the acid site densities on the char, the base site densities were also evaluated using the Boehm titration method. The base site densities are illustrated below in figure 17.

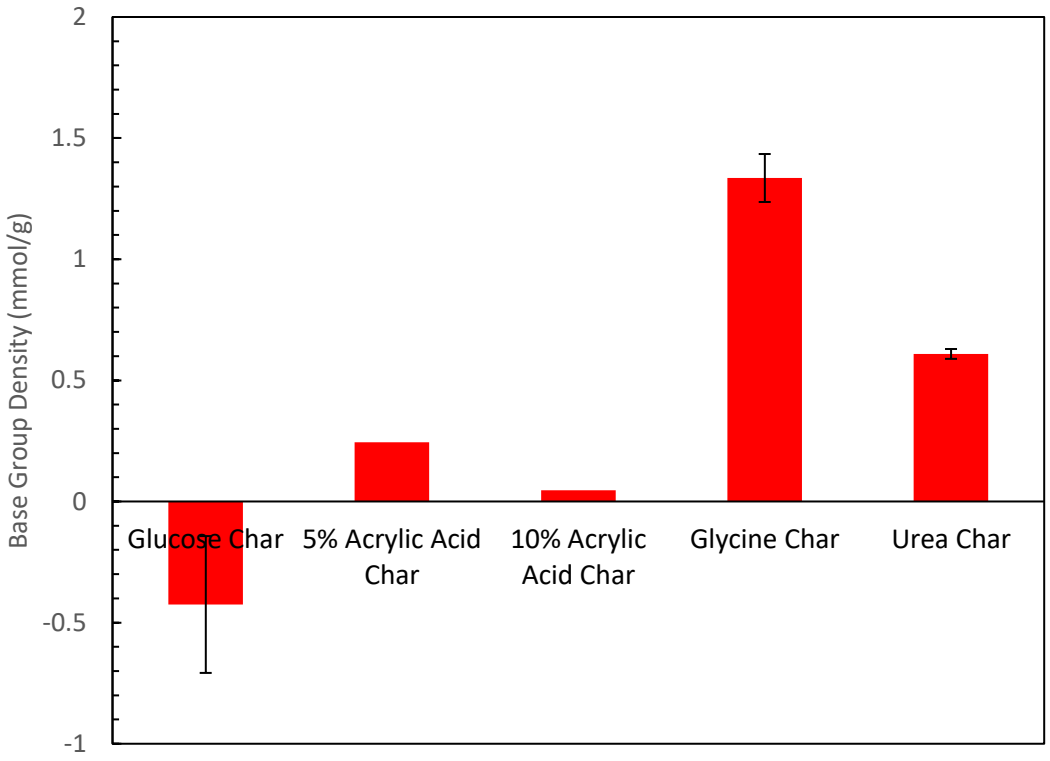

Figure 17: *Boehm titration results for glucose and modified hydrochars base sites*

In the Boehm titration, base sites were not able to be detected with the glucose char. This resulted in a negative base site density value for the glucose char, because more titrant was added than acid when acidifying the sample. This indicates that there is no to very little base present in the run glucose char samples. The titration could be rerun for the glucose char with more

sample/more precise titration in order to better determine the value for this char. The modified chars were able to successfully be analyzed with the titration method. Both the acrylic acid chars had small amounts of detected bases sites (<0.25 mmol/g). This is consistent with expectations because of the acidic starting conditions. Both the glycine and urea chars had significantly more base sites than the acrylic acid chars. The urea char had around 0.6 mmol/g and the glycine char has around 1.3 mmol/g total base sites. This success in integrating base sites provides confidence in the ability to selectively synthesize chars with desired macroscopic characteristics using different starting materials.

A summary of total acid and base sites, as well as the group breakdown is presented below in table 1.

Table 1: *Summary of Boehm titration results for each char*

Char	Total Acid Sites (mmol/g)	Total Base Sites (mmol/g)	Strongest Acid (Carboxylic)	Medium Acids (Lactonic)	Weak Acids (Phenolic)	Acid/Base Ratio
Glucose	5.2 ±0.4	-0.4 ±0.3	0.9 ±0.1	1.3 ±0.3	3.0 ±0.5	NA
5% Acrylic Acid	5.0 ±0.02	0.2 ± 0.0	1.7 ±0.1	2.7 ±0.2	0.5 ±0.2	20.4
10% Acrylic Acid	6.1 ±0.1	0.05 ±0.0	2.7 ±0.1	1.6 ±0.5	1.8 ±0.5	133.3

Glycine	3.7 ±0.2	0.6 ±0.02	0.7 ±0.1	1.0 ±0.3	1.9 ±0.3	2.2
Urea	3.0 ±0.0	1.3 ±0.1	0.8 ±0.0	2.0 ±0.3	0.1 ±0.3	6.0

Zeta Potential

With understanding of the acid and base sites on the different chars established, the zeta potential of the chars were investigated. The experimental zeta potentials of all chars can be seen graphed below in figure 18. The zeta potential of the glucose char is in between that of the acid and base chars, which makes sense in relation to the total acid and base group properties of all the chars. The one region that is not fully explained by the titration and NMR data for the glucose char is the positive region. The glucose zeta potential contains a large region of positive zeta potential, however the titration did not detect any base sites. This could be due to various different factors. The titration may need to have greater resolution in order to detect the small number of base sites present, or other phenomena in zeta potential measurements, such as binding of counter-ions, could have contributed to creating the positive region.

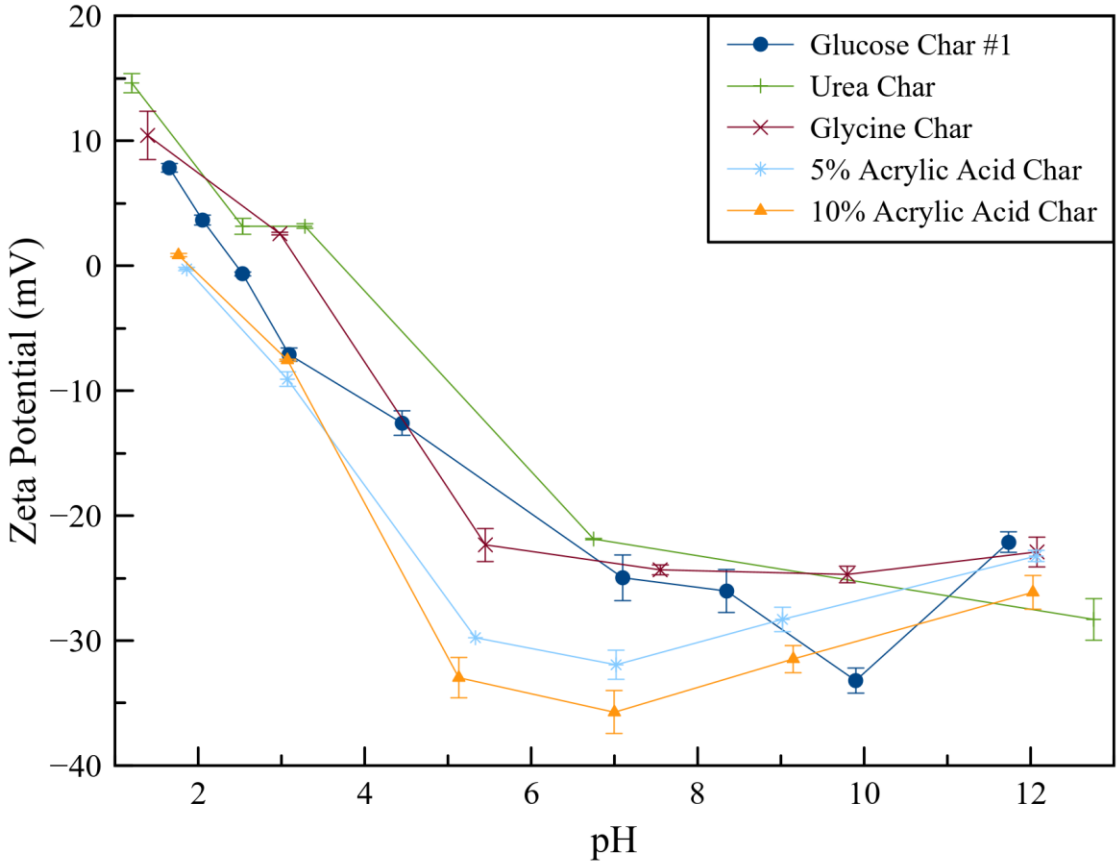

Figure 18: *Zeta potential measurements for all chars over a pH range of ~1-12*

The main trend in the zeta potential is the difference between the acid and base chars. The acrylic acid chars have lower minimum zeta potential values compared to the glucose char, and between the two acid chars, the 10% acrylic acid char has the lowest minimum value. The acid chars also have little to no positive zeta potential region, which correlates with the little detected base sites and large amount of acid sites. The base chars have higher minimum zeta potential values compared to the glucose char. In comparison to the glucose char, the base chars have larger positive region, which correlates with the larger amount of base sites and comparably smaller amount of acid sites.

From the data, there are three main characteristics that can help to characterize the zeta potential data for each char. These three characteristics are the minimum zeta potential value, point zero charge (PZC), and the acidic region slope (~pH1 to pH~7). Below in table 2, these values are summarized for each char extracted/estimated from the data. When using the mathematical model, these characteristics were used to try to guide how to change parameters in order to create a fit for the experimental data.

Table 2: *Summary of zeta potential curve characteristics for each char*

Chars	Minimum (mV)	PZC (pH)	Slope
Glucose	-33.2	2.48	-6.0
5% Acrylic Acid	-31.9	1.75*	-8.5
10% Acrylic Acid	-35.7	1.88	-10.0
Glycine	-24.3	3.3	-8.1
Urea	-28.3	3.75	-6.6

To gain insight into the regions of the zeta potential measurements, some of the characteristics were analyzed in conjunction with the titration data. These can be seen below in figures 19 and 20.

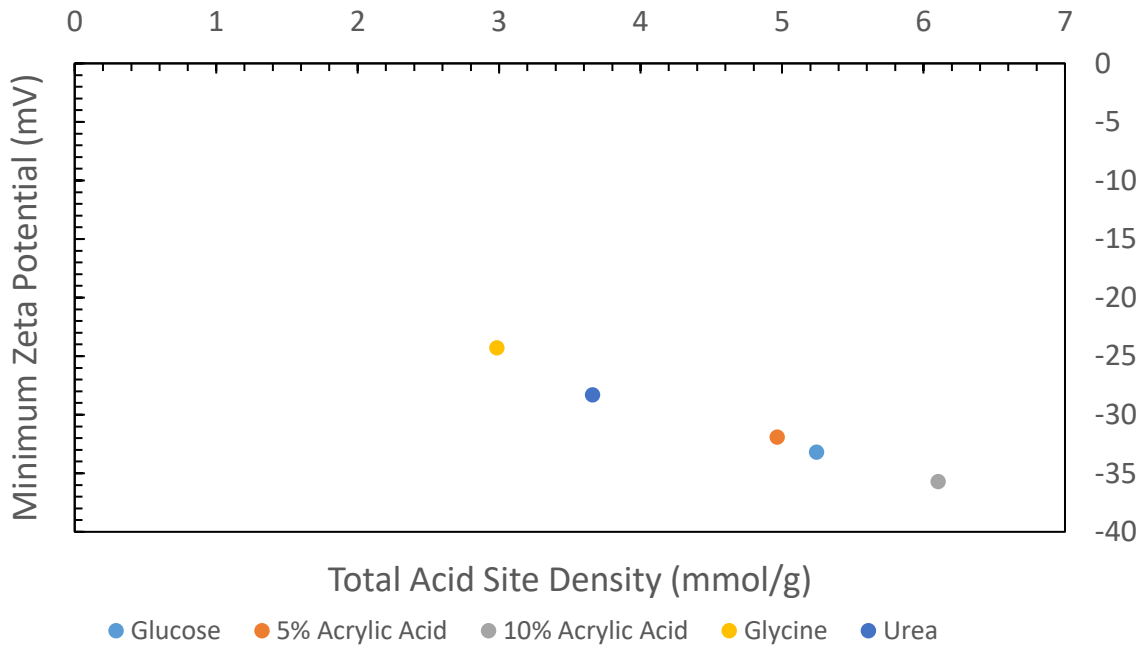

***Figure 19**: Plot of minimum zeta potential value of each curve versus the total acid site density of each char from Boehm titration (mmol/g)*

The minimum zeta potential values is correlated with the total acid site density of the char. As the acid site density increases, the minimum decreases. This is because of the function of the acid sites. As there are more acid sites to dissociate, the charge on the particle becomes stronger, which decreases the minimum value.

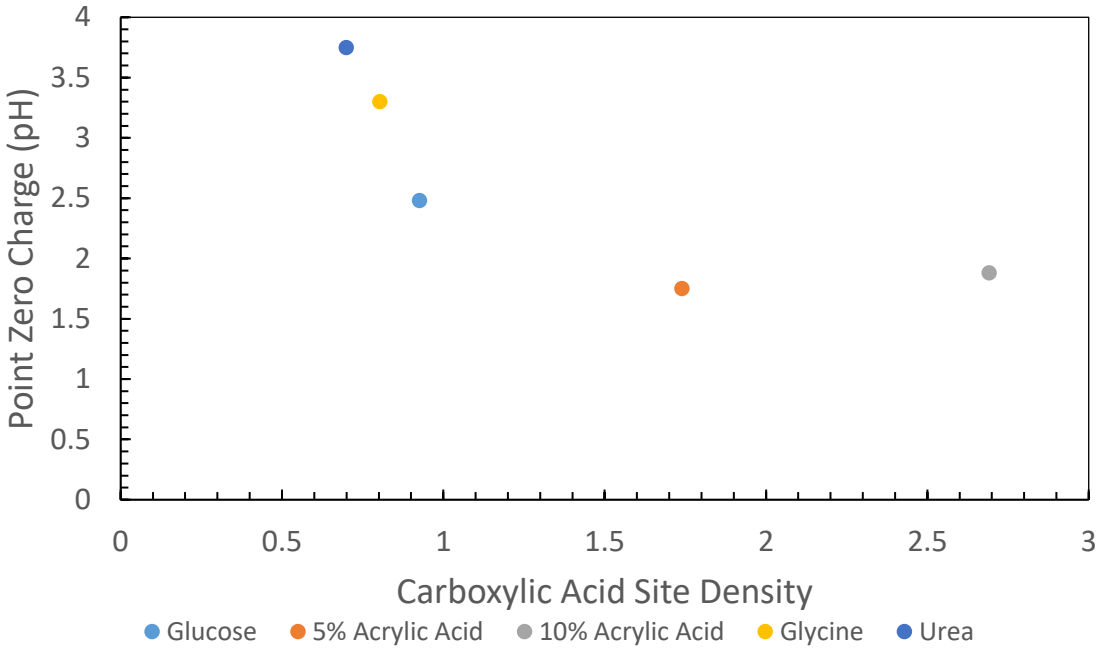

***Figure 20**: Plot of point zero charge pH versus the carboxylic acid site density for each char (mmol/g)*

Similarly, the point zero charge is correlated with the carboxylic acid site density. As the density of carboxylic acid sites increases, the point zero charge decreases. This is similar to the minimum zeta potential because as the acid sites increase, it necessitates a higher pH in order to protonate the surface of the char and give the char a neutral surface charge. The insights into some of what affects these different characteristics of the zeta potential curve were used in order to determine how some of the model parameters were adjusted.

Mathematical Model

The mathematical model was first used to attempt to create fits for the glucose char. As shown in the background calculation section of this report, the model has many different adjustable parameters that could help to fit to the experimental data. The model was initially ran

with conservative estimates for most parameters in order to see how the model fit the data with no adjustments. The initial run can be seen below in figure 21. The model was run using NMR data to see how well the data provided from that analysis could help to predict the experimental char properties.

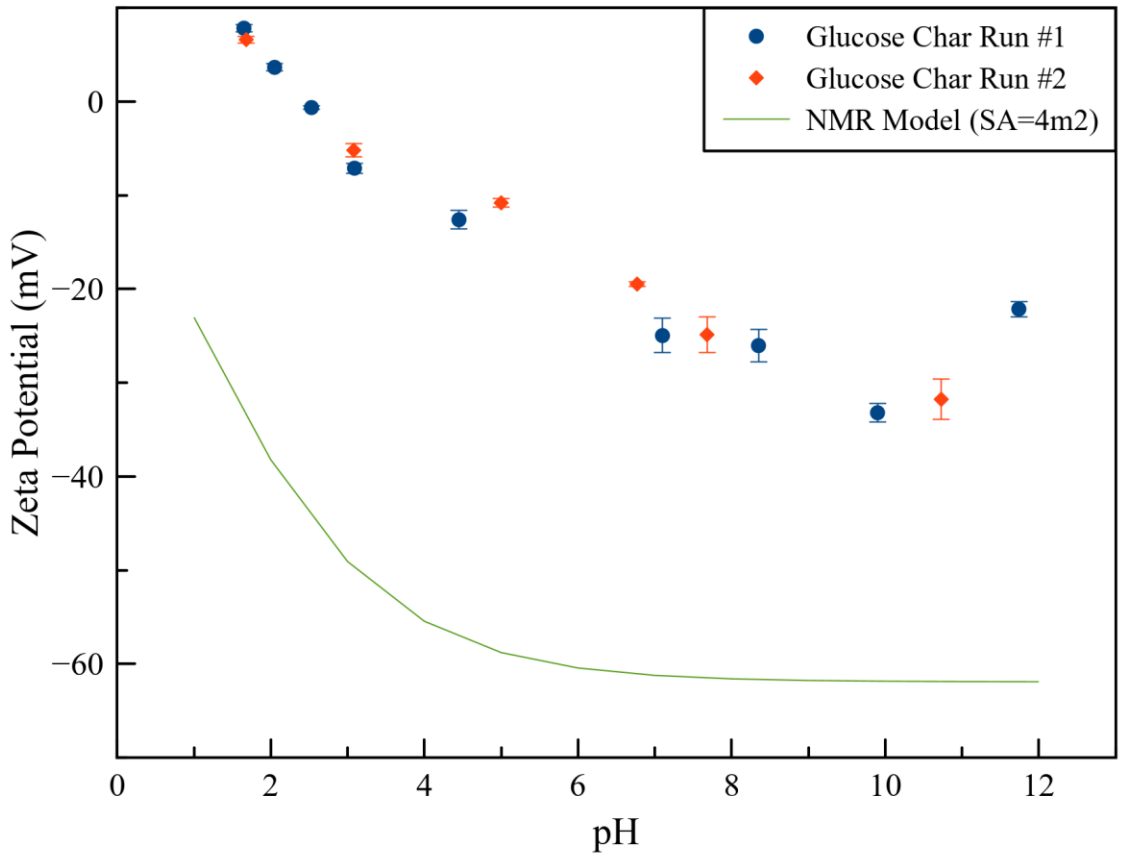

Figure 21: *Initial mathematical model zeta potential curve compared to experimental glucose results*

The model represents the general trends of the experimental data, but does not provide a good fit with unadjusted parameters. It has a much lower minimum zeta potential value (-61.9mV) compared to the experimental results (-33.2 mV). Since the unadjusted model could not

provide a good fit, some parameters within the model were adjusted to create a better fit with the data.

Surface Area

One of the parameters governing the density of acid sites on the surface of the char particle is the surface area of the particle. In order to understand the surface area of the glucose char, physisorption of both N_2 and CO_2 was carried out with the char. The results of the physisorptions can be seen below in table 3.

Table 3: *BET surface of glucose hydrochar with N2 and CO2 as adsorbents*

Sample	**Adsorbent**	**Temperature (K)**	**BET Surface Area (m2/g)**
Glucose hydrochar	N2	77	1.0
	CO2	273	46

One of the main differences in these two adsorptions is the temperature which they are run at, 77 K for N_2 and 273 K for CO_2. The low temperature of the N_2 adsorption can cause issues when measuring microporous solids such as coals and activated carbons [30]. The low temperatures can kinetically restrict access to micropores in the particle [30]. With the warmer temperature of CO_2, this problem can be avoided and will interact chemically more than N_2 [30]. These results were both tested in the model to examine how the fits differ. In experimental zeta potential measurements, it is expected that when a char particle is in water it will swell/expand

increasing the surface area available. This would indicate we expect the CO_2 value to create a better fit within the model. Higher values were also tested to examine the effect on the model, although these values may be unrealistic compared to the actual surface area of the char. The model results can be seen in figure 22 below.

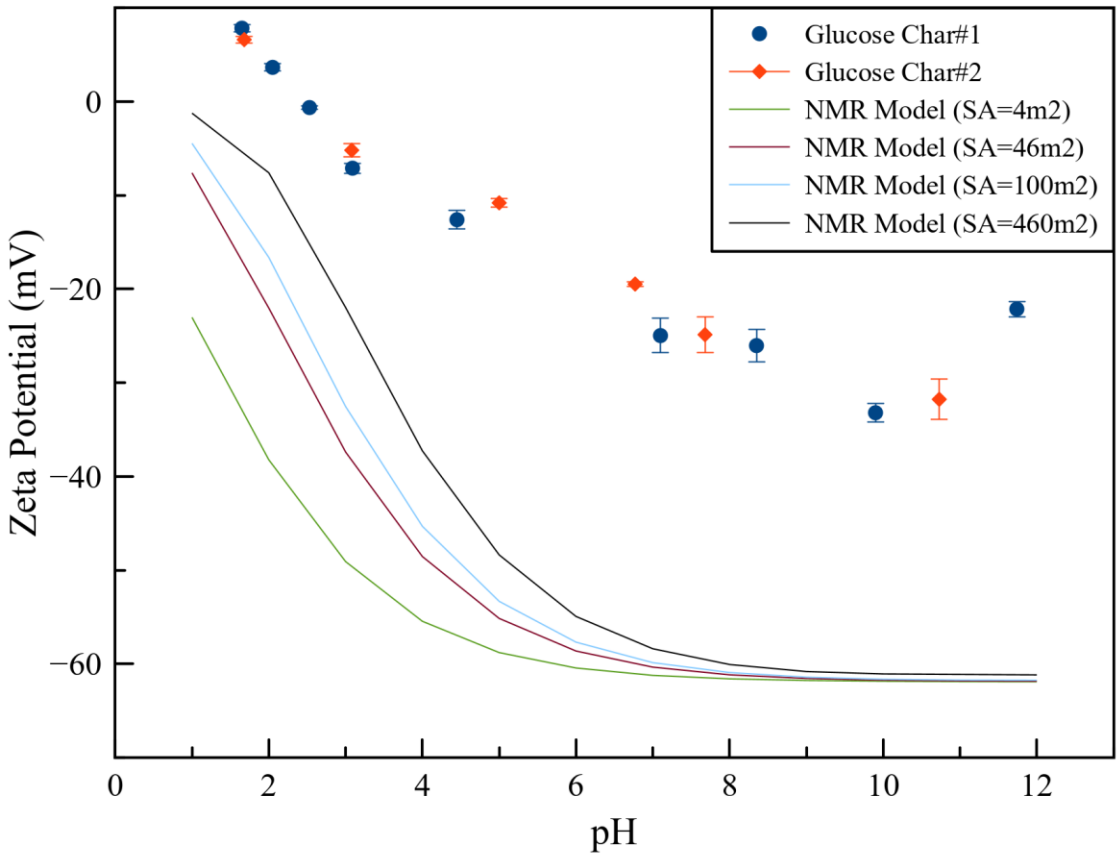

Figure 22: *Effect of surface area on zeta potential model*

As expected, the value from the CO_2 test shifts the model closer to the experimental data. The unrealistic higher values show that increasing the surface area does shift the model values upwards, but an unrealistic very high surface area would be necessary to continue to shift the

model to the experimental data. With the surface area now corrected to the CO_2 experimental value, further parameters were adjusted to fit the model to the data.

Particle Size

Another parameter within the model that was examined was the particle size. The results of the model can be seen in figure 23.

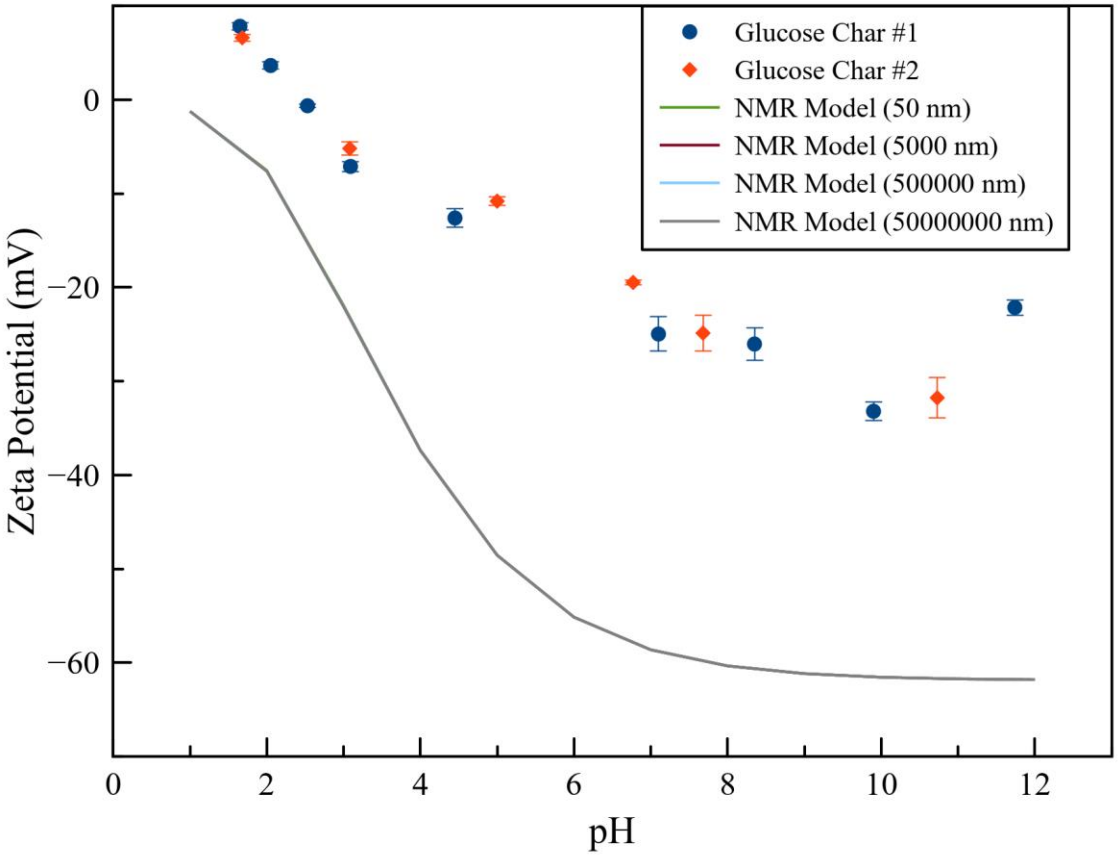

Figure 223: *Effect of particle size on zeta potential model*

This analysis indicates that the particle size has very negligible on the model and does not have to be adjusted in order to create a fit.

Slip Plane

The next parameter adjusted within the model is the slip plane. The shifting of the slip plane defines where in the solution the zeta potential is calculated away from the particle. As described earlier, Yamaguchi et al. [28] used a slip plane shift of 0.5 – 2 nm in order to create a fit for the experimental data. A similar shift was carried out to examine the effect on the hydrochar model. The results of the shift can be seen below in figure 24.

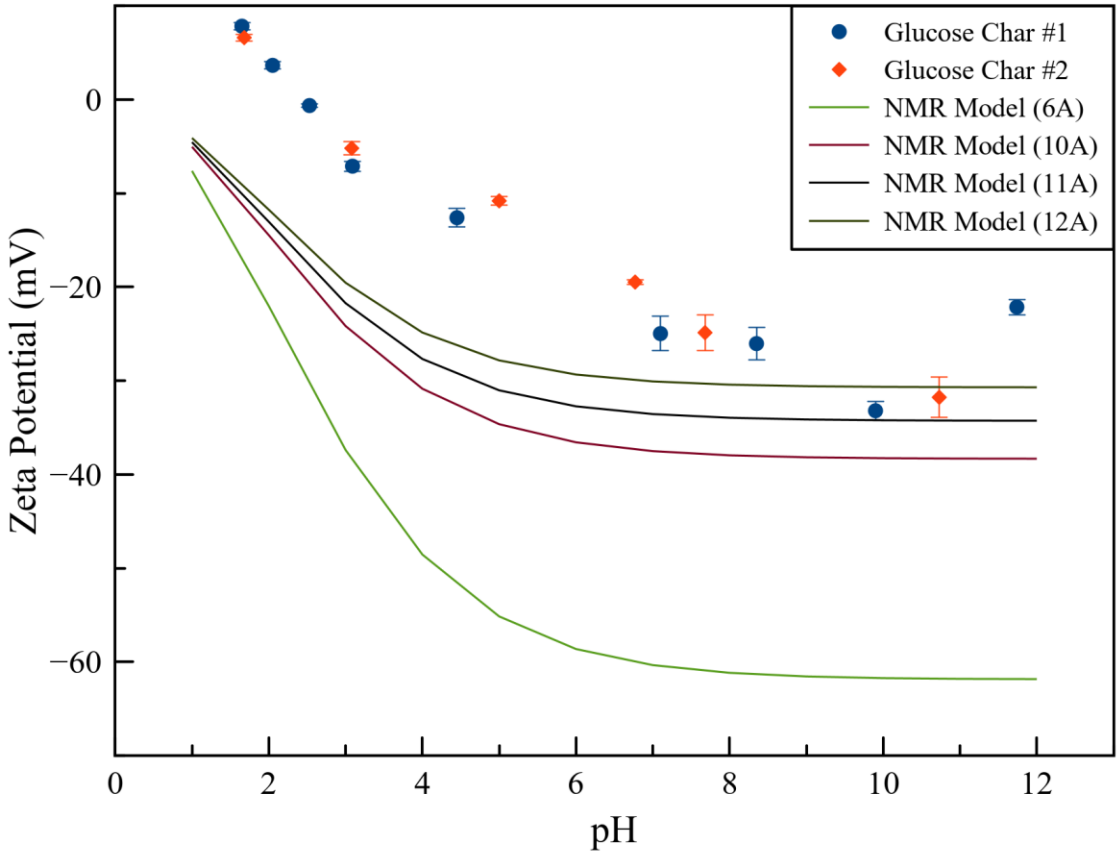

Figure 234: *Effect of slip plane location on zeta potential model*

This change in the slip plane parameter has the greatest effect on the model fit of the tested parameters. A shift of the slip plane up to about 11- 12 Å (1.1-1.2 nm), increases the

minimum value for the model. The minimum value of the 12 Å curve is -30.7 mV, where the minimum experimental value between both glucose char runs was -33.2 mV. This parameter adjustment completes one of the model fitting objectives of raising the basic range to the minimum of the experimental data. One of the main differences still to be resolved within the model is the positive region present in the experimental data, which is not present in the model.

Base Groups

In order to introduce a positive region into the model, it was necessary to introduce base groups into the model. The one issue with adding base groups is that none were detected from the Boehm titration method. This could be due to the lack of resolution within the titration method carried for very low base site densities. In order to take this into account, a very small amount of weak base (~pKa 10) was added into the model. The amount of base groups was kept at a low density in order for it to be undetected by the titration method (<0.005 mmol/g). Two different base densities were run (1:300 Base per char molecules, and 2:300). The results can be seen below in figure 25.

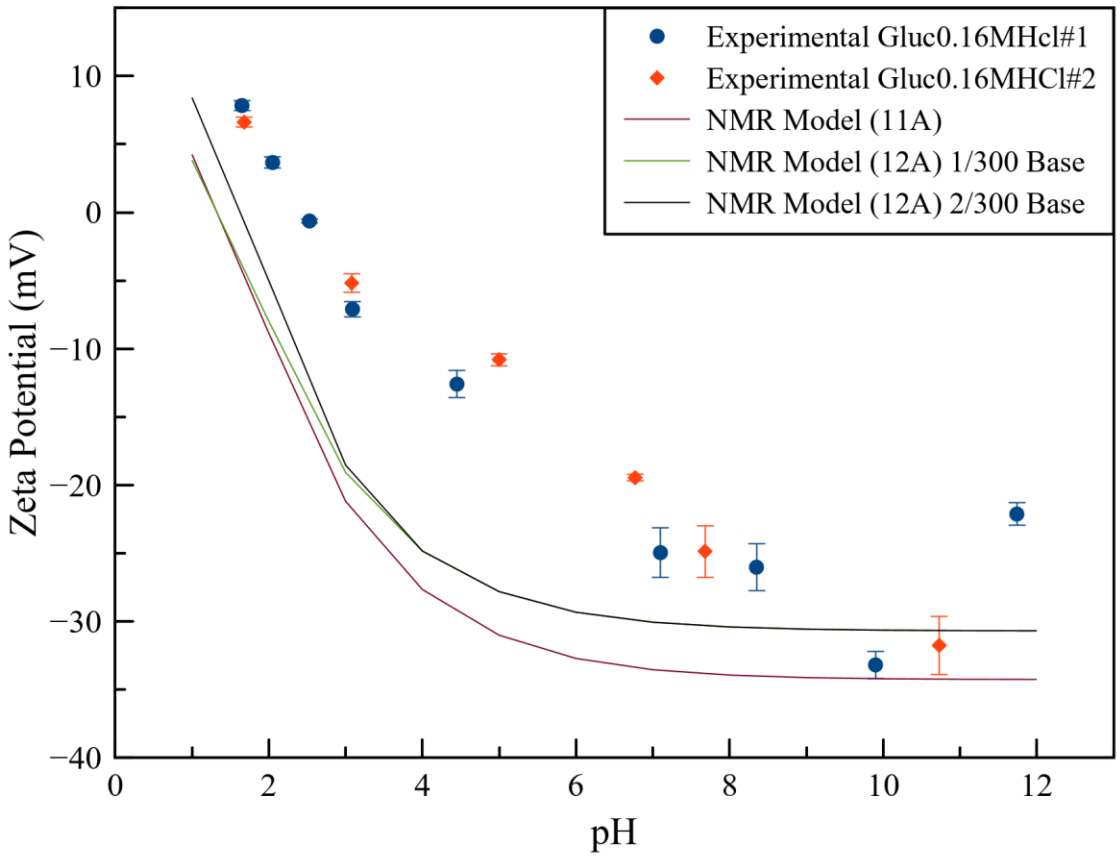

Figure 245: *Effect of addition of base groups to zeta potential model*

The addition of a small amount of base groups introduces the positive region into the model curve that is present in the experimental values. This creates a better fit for the model with experimental data without being unreasonably different from the titration results. The small increase in acid site density with additional base also shifts the point zero charge, which moves it closer the PZC of the experimental data.

Carboxylic pKa

Since carboxylic acid is the most acidic functional group taken into account in the model and it is a large factor in the point zero charge, it was expected to have a great effect on the

model curve. Determining the pKa to use for carboxylic acid in the model is difficult due to the varying versions present in the model, as well as the unknown experimental conditions of each group. Below in figure 26 is a graph of different benzoic groups along with the pKa of each group.

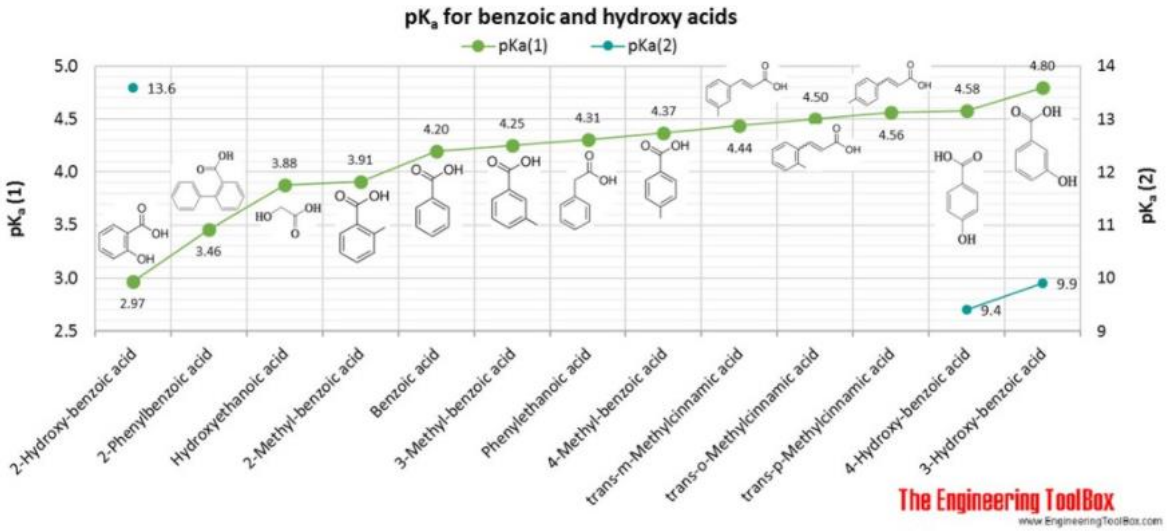

Figure 256: *Graph of various benzoic acids pKa values [31]*

Two of these groups are present in the NMR structure; the 2-Hydroxy-benzoic acid (pKa of 2.97) and 3-Hydroxy-benzoic acid (pKa 4.8). There is also a carboxylic group on a furan ring present in the molecule. The large difference in these groups as well as the possible surroundings and additional groups present in the actual molecular structure make it difficult to select a pKa value. In Delahaye et al. with a similar glucose char, it was determined that "the pKa of these acid groups must be greater than approximately 3" due to the presence of mostly protonated forms of carboxylic acid [13]. In previous studies, it was also determined for some basic hydrochars the carboxylic group's dissociation constant was around 4.4-5.3 [23]. Based on these findings, the model was tested with values from the higher range pKa (4.3, 4.8, 5). These values

may not be the most accurate reflection of the chemical environment, but better qualification of the groups and the experienced pKa would be necessary to fully understand how/if it differs. The results can be seen below in figure 27.

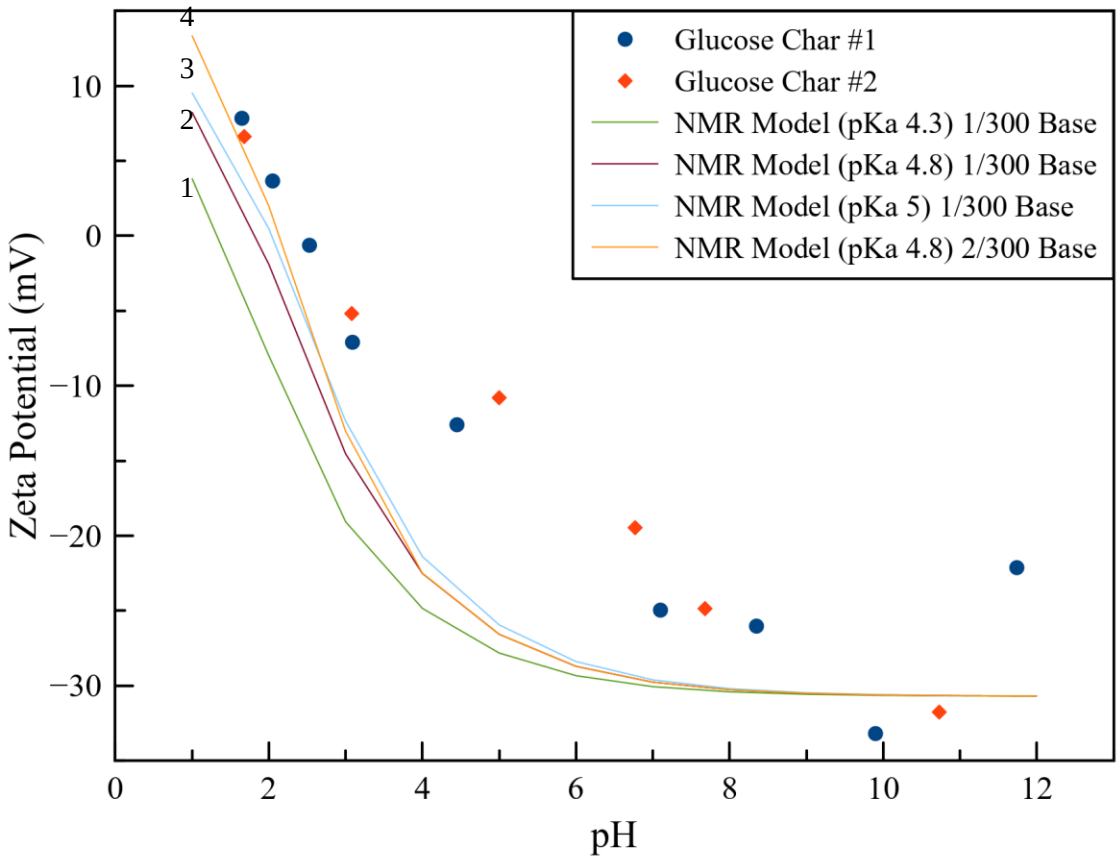

Figure 267: *Effect of changing carboxylic acid pKa on zeta potential model*

The increase in the pKa value of the carboxylic acid helps the model to fit the experimental data. These fits qualitatively appear to have a good fit for most of the experimental data. To see which parameters, create best fits the important regions of the experimental data, each curves properties are presented below table 4.

Table 4: *Experimental zeta potential curve characteristics values compared to models*

Curves	Minimum (mV)	Pzc (pH)	Slope
Glucose	-33.2	2.48	-6.0
NMR Model Carbox pKa 4.3, 12 A shift 1/300 Base	-30.7	1.40	-5.7
NMR Model Carbox pKa 4.8, 12 A shift 1/300 Base	-30.7	1.91	-6.3
NMR Model Carbox pKa 5, 12 A shift 1/300 Base	-30.7	2.09	-6.5
NMR Model Carbox pKa 4.8, 12 A shift 2/300 Base	-30.7	2.21	-7.2

The increase in base groups resulted in a larger slope but a closer PZC, while the increase in pKa resulted in a closer slope but a greater separation from the PZC. From this data points the 5pKa and 1/300 base and 4.8 pKa and 2/300 base curves are the best fit for the model. With

further small adjustments to the model, more precise fits could be established, but these curves have close agreement in the three main values of the zeta potential curve.

The one area where the model has trouble fitting is the middle of the curve in the acidic region. This could be due to the model not being able to accurately represent all physical and chemical phenomena besides dissociation occurring in that region. The other characteristic of the experimental data that is missing is the increase in zeta potential in the basic region. The potential model is not able to take this into account without further modification for that specific region, but still represents the general trends of dissociation on the surface of the particle besides in that range.

NMR vs Titration

With a good model fit established using the NMR group breakdown, the titration data was run using the same parameters to see whether one data set creates a better fit than the other. If the titration data is able to create a better or similar fit as the NMR, it would allow for predicting macroscopic properties for chars that have not been extensively NMR analyzed. This would allow for similar confidence predictions with a significantly less complex and expensive characterization method. A comparison can be seen in the curves below in figure 28.

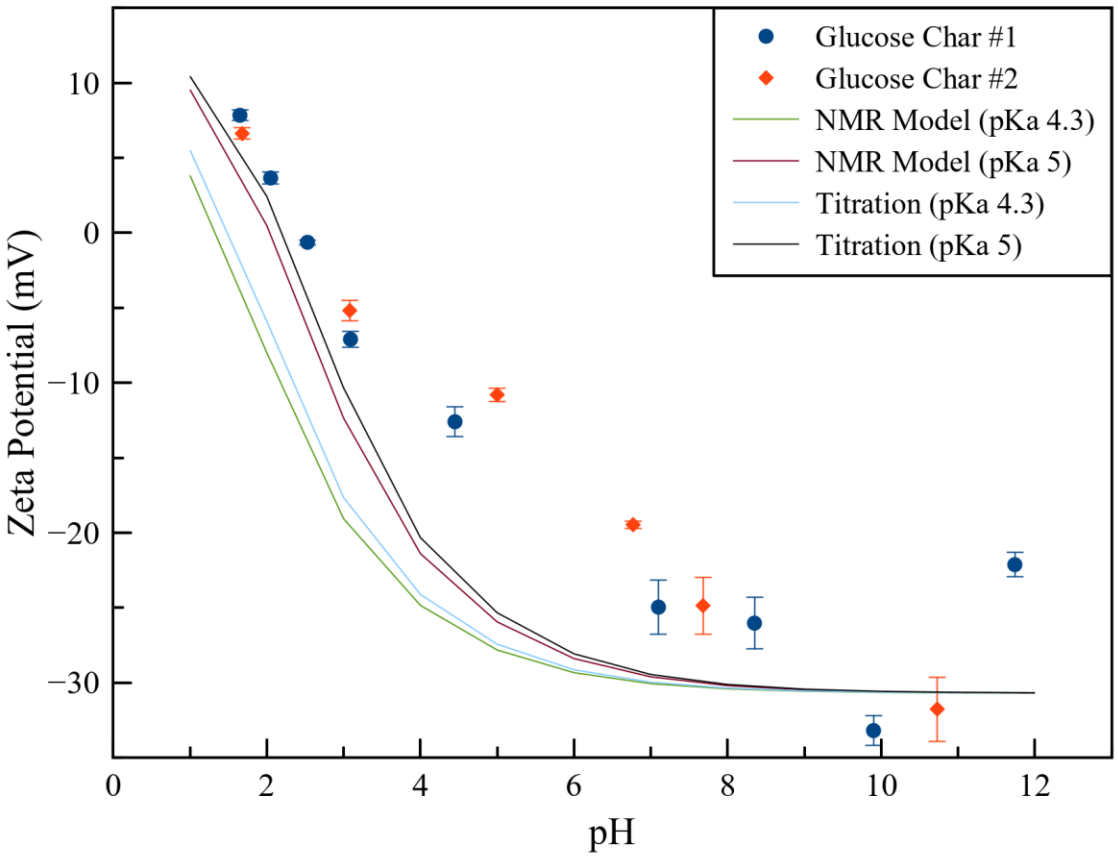

Figure 278: *Zeta potential model, NMR site data comparison to titration site data*

The difference between the curves for titration data and NMR data is minimal. The slight difference between the two curves is most likely from the decreased number of carboxylic groups within the model. The minimal difference illustrates that the NMR and titration data are a good comparison and that the data are mostly interchangeable within the mathematical model. Because the data from both are comparable, the titration data of the modified chars can be put into the model to determine fits.

Modified Chars

The site density of the model was altered to match the titration data of each modified char. This included changing the base site density, which necessitated modifying the base pKa parameter in order for the model to run correctly. The base parameters used for each char, along with the curve fit graphs can be found in Appendix C. A summary of the main characteristics of the basic fit graphs with comparison to experimental data for each char can be seen below in table 5.

Table 5: *Zeta Potential curve characteristics for each model fit*

Char Fit	Minimum (mV)	PZC	Slope	Slip Plane (nm)	Carboxylic pKa
Glucose	-30.7	2.09	-6.5	1.2	5
5% Acrylic Acid	-30.7	1.13	-6.1	1.1	5
10% Acrylic Acid	-34.3	1.22	-7	1.1	4.3
Glycine	-24.7	1.67	-5.6	1.4	5
Urea	-27.5	1.67	-6.6	1.3	5

Some curves required an increase or decrease in the slip plane in order to get a better fit close to the correct minimum value. The 10% Acrylic Acid curve fit better with a carboxylic acid pKa of 4.3 than with a pKa of 5 like the other curves. This could be due to the greater site density on the 10% acrylic acid char compared to the other chars. With these values extracted from the model plots, three parity plots were created in order to compare the experimental values to the model values. These plots can be seen below in figures 29, 30, and 31.

As shown in the figure 29, the point zero charge of the model did not correlate very well to the experimental value for most chars. Most of the chars PZC were underestimated by the model. This is most likely due to further model adjustment needed for modified chars, as well as the model not completely mirroring the physical phenomena within the experiment. Modified chars may not be perfectly described by the model adjustments created for the glucose char. Further analysis of theses chars, including more surface area measurements, NMR structure analysis, and pKa characterization, could help to understand how best to adjust the NMR mathematical model for chars based on their various characteristics. The glucose char model fit had the closest PZC to the experimental value. The model was optimized for this char and the glucose char has least amount of basic groups, which cause a problem when optimizing for modified chars.

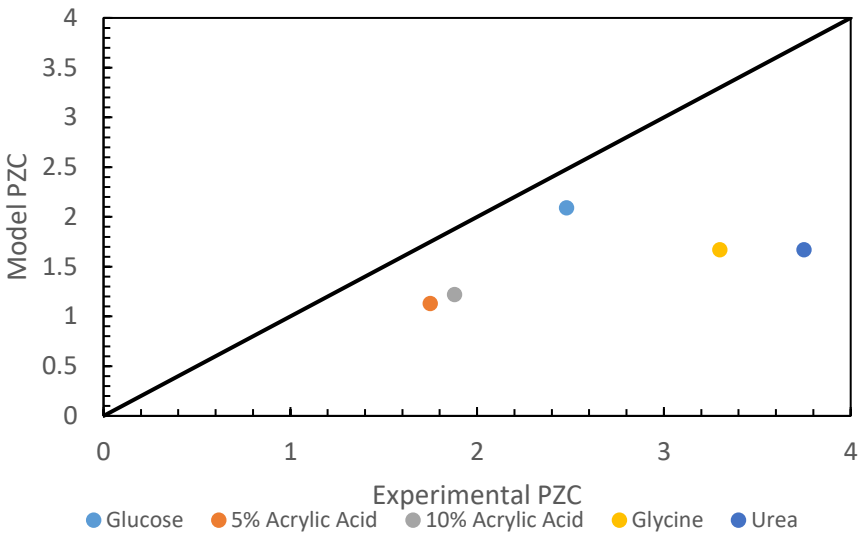

Figure 289: *Parity plot for point zero charge*

Compared to the PZC, the slope is better fit between the model and experiment as shown in figure 30. The modified char models are further from the experimental than that of the glucose char, similar to the PZC parity plot.

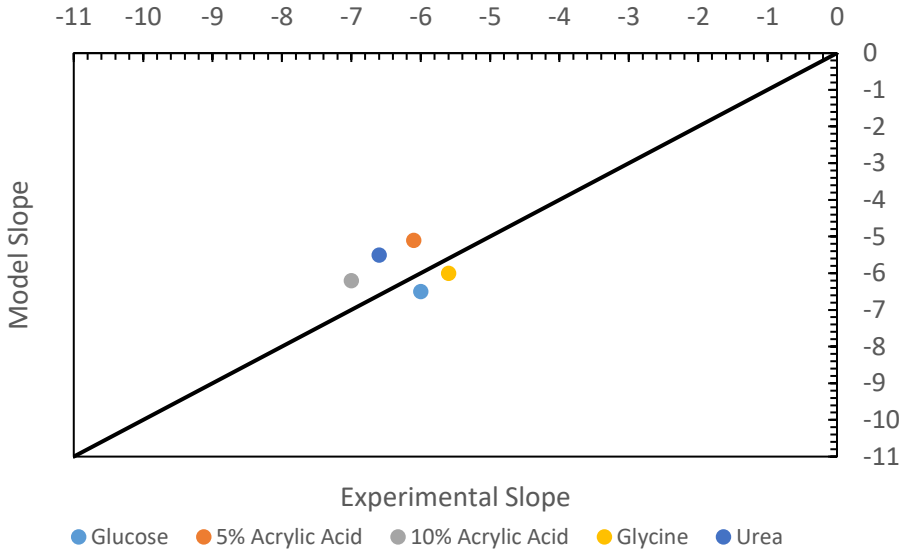

Figure 3029: *Parity plot for acidic region slope*

As shown in figure 31, the minimum model values are well fit to the experimental values. This is due to the slip plane shift which helps to increase the minimum value to around the experimental values. Also, this is only dependent on the dissociation of acid sites, which is well defined by both the titration and NMR The slope and PZC are dependent on both the acid and base site density of the char. The uncertainty of both the acid and base pKas and site density, causes more discrepancy in the model compared to the glucose char, which has a very small amount of base groups.

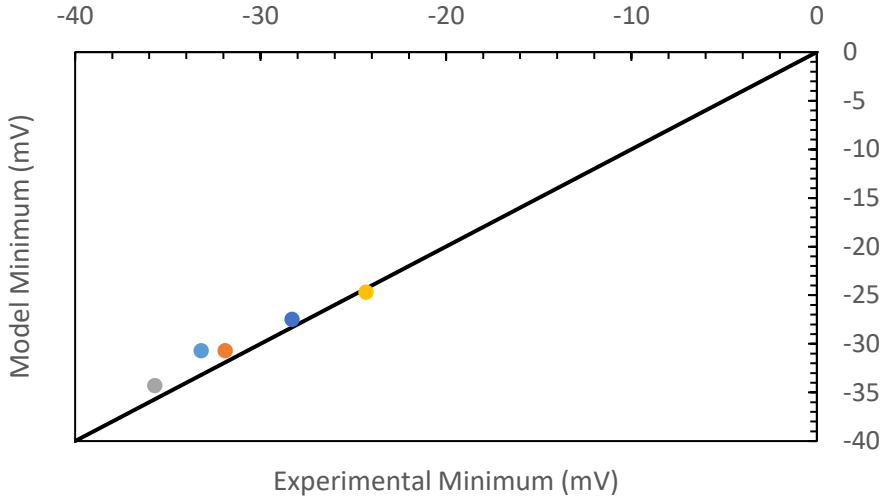

Figure 301: *Parity plot for minimum zeta potential value*

Conclusions/Recommendations

Hydrochars have the potential to be a sustainable source of carbon materials that take advantage of waste feedstocks. Understanding the chemical structure of char is important for designing chars for specific applications. NMR can be used to understand and develop a model molecular structure of the char. The Boehm titration method can also be used to gain some knowledge of char's structure, specifically the surface acid and base sites. The comparison between the NMR structure created by the group at Brandeis and the literature structures to the experimental titration data provide further confidence in the NMR structure being a useful prediction for the actual char structure. With this confidence in the NMR structure and the titration data from hydrochar, the ability of both datasets were tested to see whether they can predict macroscopic properties (zeta potential). With some adjustments to the zeta potential model, the NMR model structure was able to create good, although not perfect fits to experimental datasets. This illustrates the ability to predict to a certain extent the macroscopic properties for adsorptive phenomena from a hypothetical structure. The titration data was also examined in the prediction model. Even with the uncertainty of pKa of groups and imprecise group breakdown that comes with the Boehm titration, the titration data created as good a fit to the experimental data as the NMR. These findings gave us the ability to predict the macroscopic properties, without needing the NMR molecular structure for complete confidence. The ability to predict macroscopic properties even without the NMR, opens the opportunity to understand adsorption phenomena and predict how certain modified chars may perform in adsorption testing. This prediction ability along with the matching of NMR and Boehm titration data can help to further provide insight into modifying hydrochars for certain applications and understanding the possible macroscopic behaviors.

Recommendations

For future research, a greater dataset of NMR structures could be created for modified hydrochars. This would provide further evaluation of the comparison between the NMR and titration data. It can help to further validate the ability to create a good fit for macroscopic properties from NMR data. It may also allow better model correction for specific modified chars were some parts of the glucose model do not fit. Another recommendation is to combine this type of analysis with evaluation of adsorption capacities of modified chars. This can help to evaluate the predictive performance of the model, as well as give insight into how the data from this study allows predictions or assumptions on the applicability of chars with certain structures for certain applications, specifically adsorption.

References

1. United Nations Environment Programme (2021). Food Waste Index Report 2021. Nairobi.
2. *Fight climate change by preventing food waste*. World Wildlife Fund. https://www.worldwildlife.org/stories/fight-climate-change-by-preventing-food-waste.
3. C.A. Ramírez, E. Worrell, Feeding fossil fuels to the soil: An analysis of energy embedded and technological learning in the fertilizer industry, Resources, Conservation and Recycling 46(1) (2006) 75-93.
4. J. E. Gilley, L. M. Risse, Runoff and soil loss as affected by the application of manure, Transactions of the ASAE 43(6) (2000) 1583-1588
5. I. Bargmann, M.C. Rillig, A. Kruse, J.-M. Greef, M. Kücke, Effects of hydrochar application on the dynamics of soluble nitrogen in soils and on plant availability, Journal of Plant Nutrition and Soil Science 177(1) (2014) 48-58.
6. Y. Shi, T. Zhang, H. Ren, A. Kruse, R. Cui, Polyethylene imine modified hydrochar adsorption for chromium (VI) and nickel (II) removal from aqueous solution, Bioresource Technology 247 (2018) 370-379.
7. A.B. Brown, B.J. McKeogh, G.A. Tompsett, R. Lewis, N.A. Deskins, M.T. Timko, Structural analysis of hydrothermal char and its models by density functional theory simulation of vibrational spectroscopy, Carbon 125 (2017) 614-629.

8. K.G. Latham, G. Jambu, S.D. Joseph, S.W. Donne, Nitrogen Doping of Hydrochars Produced Hydrothermal Treatment of Sucrose in H2O, H2SO4, and NaOH, ACS Sustainable Chemistry & Engineering 2(4) (2014) 755-764.

9. M. Titirici, R. White, N. Brun, V. Budarin, D. Su, F. Monte, J. Clark, M. MacLachlan Sustainable carbon materials, Chemical Society reviews 44 (2014).

10. H.S. Kambo, A. Dutta, A comparative review of biochar and hydrochar in terms of production, physico-chemical properties and applications, Renewable and Sustainable Energy Reviews 45 (2015) 359-376

11. *Project Jining - sludge drying by terranova energy*. TerraNova Energy GmbH. https://terranova-energy.com/en/project/project-compiegne/.

12. *Official launch of the ava htc plant In relzow*. IPI.

https://ipi.ag/en/article/official-launch-of-the-ava-htc-plant-in-relzow_6

13. L. Delahaye, J.T. Hobson, M.P. Rando, B. Sweeney, A.B. Brown, G.A. Tompsett, A. Ates, N.A. Deskins, M.T. Timko, Experimental and Computational Evaluation of Heavy Metal Cation Adsorption for Molecular Design of Hydrothermal Char. *Energies (Basel)*, *13*(16), (2020) 4203–. https://doi.org/10.3390/en13164203

14. F. Fu, Q. Wang, Removal of heavy metal ions from wastewaters: A review. J. Environ. Manag. 2011, 92, 407–418.

15. K.-M. Poo, E.-B. Son, J.-S. Chang, X. Ren, Y.-J. Choi, K.J-. Chae, Biochars derived from wasted marine macro-algae (Saccharina japonica and Sargassum fusiforme) and their potential for heavy metal removal in aqueous solution. J. Environ. Manag. 2018, 06, 364–372.

16. M. Karnib, A. Kabbani, H. Holail, Z. Olama, Heavy Metals Removal Using Activated Carbon, Silica and Silica Activated Carbon Composite; Elsevier Ltd.: Amsterdam, The Netherlands, 2014; Volume 50, pp. 113–120.

17. D.P. Bezerra, R.S. Oliveira, R.S. Vieira, C.L. Cavalcante, D.C.S. Azevedo, Adsorption of CO2 on nitrogen-enriched activated carbon and zeolite 13X, Adsorption 17(1) (2011) 235-246.

18. A. Chuntanapum, Y. Matsumura, Formation of tarry material from 5-HMF in subcritical and supercritical water, Industrial & engineering chemistry research 48(no. 22) (2009) 9837- 9846

19. K.G. Latham, M.I. Simone, W.M. Dose, J.A. Allen, S.W. Donne, Synchrotron based NEXAFS study on nitrogen doped hydrothermal carbon: Insights into surface functionalities and formation mechanisms, Carbon 114 (2017) 566-578.

20. A.B. Brown, G.A. Tompsett, B. Partopour, N.A. Deskins, M.T. Timko, Hydrochar structural determination from artifact-freer Raman analysis. Carbon 167, 378-387.

21. M. Uchimiya, L.H. Wartelle, K.T. Klasson, C.A. Fortier, I.M. Lima, Influence of Pyrolysis Temperature on Biochar Property and Function as a Heavy Metal Sorbent in Soil. Journal of Agricultural and Food Chemistry 59(6) (2011) 2501-2510.

22. S.L. Goertzen, K.D. Theriault, A.M. Oickle, A.C. Tarasuk, H.A. Andreas, Standardization of the Boehm titration. Part I. CO_2 expulsion and endpoint determination. Carbon 48(4) (2010) 1252-1261.

23. N. Saha, A. Aba, M.T. Reza, Effect of hydrothermal carbonization temperature on pH, dissociation constants, and acidic functional groups on hydrochar from cellulose and wood. Journal of Analytical and Applied Pyrolysis 137 (2019) 138-145.
24. N. Saha, K. McGaughy, M.T. Reza, Elucidating hydrochar morphology and oxygen functionality change with hydrothermal treatment temperature ranging from subcritical to supercritical conditions. Journal of Analytical and Applied Pyrolysis 152 (2020).
25. Israelachvili, J.N. Intermolecular and Surface Forces; Academic press: Cambridge, MA, USA, 2011.
26. D.C. Grahame, The Electrical Double Layer and the Theory of Electrocapillarity. Chemical Reviews 41(3) (1947) 441-501.
27. R. Herrada Garcia, M. Perez Corona, R. Shrestha, S. Pamukcu, E. Bustos, Electrokinetic Remediation of Polluted Soil Using Nano-materials: Nano-iron Case. Evaluation of Electrochemical Reactors a New Way to Environmental Protection, Research Signpost (2014).
28. A. Yamaguchi, M. Kobayashi, Quantitative evaluation of shift of slipping plane and counterion binding to lysozyme by electrophoresis method. Colloid and Polymer Science 291 (2016) 1019-1026.
29. D.P. Bezerra, R.S. Oliveira, R.S. Vieira, C.L. Cavalcante, D.C.S. Azevedo, Adsorption of CO2 on nitrogen-enriched activated carbon and zeolite 13X, Adsorption 17(1) (2011) 235-246
30. J. Garrido, A. Linares-Solano, J.M. Martin-Martinez, M. Molina-Sobia, F. Rodriguez-Reinoso, R. Torregrose, Use of nitrogen vs. carbon dioxide in the characterization of activated carbons, Langmuir 3(1) (1987) 76-81.

31. *Phenols, alcohols and carboxylic acids - pKa values*. Engineering ToolBox. https://www.engineeringtoolbox.com/paraffinic-benzoic-hydroxy-dioic-acids-structure-pka-carboxylic-dissociation-constant-alcohol-phenol-d_1948.html.

32. A. Yamaguchi, M. Kobayashi, Quantitative evaluation of shift of slipping plane and counterion binding to lysozyme by electrophoresis method. Colloid and Polymer Science 291 (2016) 1019-1026.

33. D.P. Bezerra, R.S. Oliveira, R.S. Vieira, C.L. Cavalcante, D.C.S. Azevedo, Adsorption of CO2 on nitrogen-enriched activated carbon and zeolite 13X, Adsorption 17(1) (2011) 235-246.

34. J. Garrido, A. Linares-Solano, J.M. Martin-Martinez, M. Molina-Sobia, F. Rodriguez-Reinoso, R. Torregrose, Use of nitrogen vs. carbon dioxide in the characterization of activated carbons, Langmuir 3(1) (1987) 76-81.

35. *Phenols, alcohols and carboxylic acids - pKa values*. Engineering ToolBox. https://www.engineeringtoolbox.com/paraffinic-benzoic-hydroxy-dioic-acids-structure-pka-carboxylic-dissociation-constant-alcohol-phenol-d_1948.html.

36. M.A. Islam, M.S.H Limon, M. Romic, et al. Hydrochar-base soil amendments for agriculture: a review of recent progress, Arab J Geosci 14(102) (2021).

Appendix

Appendix A: Titration Plots and Data

Table 6: Surface Areas for Literature Structures Used in Surface Site Calculation

Literature Structure	Surface Area (m^2/g)
Model 1	2018.067
Model 2	1305.58
Model 3	790.821

Example Titration Plots:

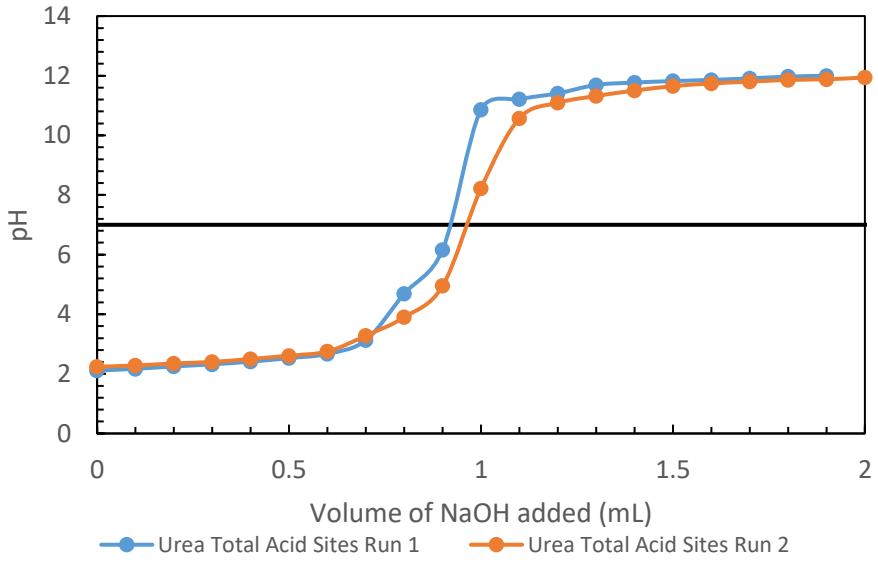

Figure 312: *Urea total acid site titration plot (NaOH reaction base)*

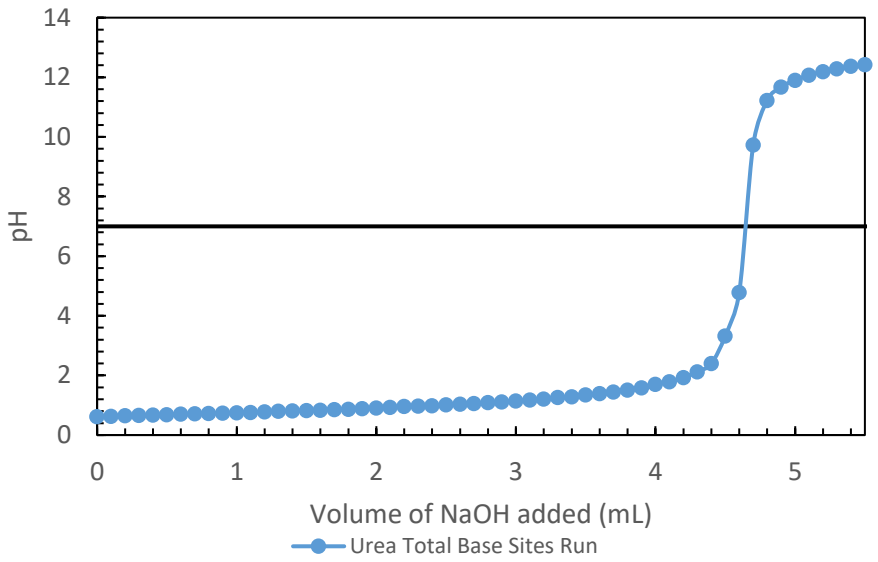

Figure 323: *Urea total base site titration plot (HCl reaction base)*

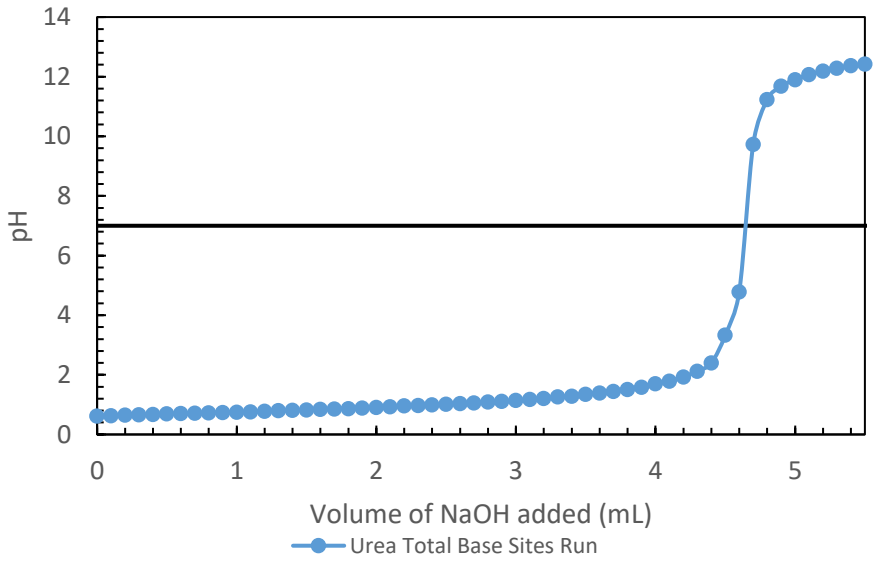

Figure 334: *Urea lactonic and carboxylic site titration plot (Na2CO3 reaction base)*

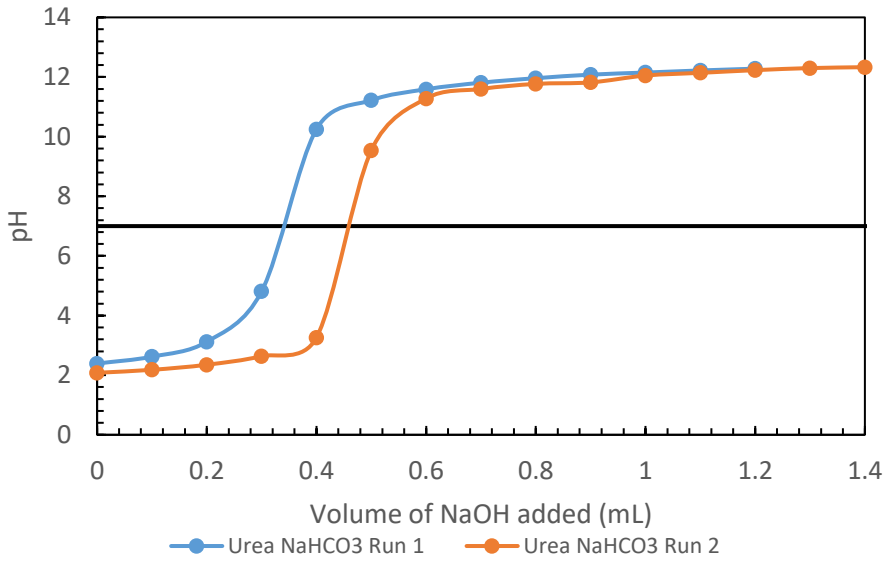

Figure 345: *Urea carboxylic site titration (NaHCO3 reaction base)*

Appendix B: MatLab Code

```
%>>>>>>>>>>>>>>>>>>>>particle size <<<<<<<<<<<<<<<<<<<<
R2 = 5000; % radius nm
% >>>>>>>>>>>>>>> dielectric constant <<<<<<<<<<<<<<<
e0 = 8.85e-12; % e0--vacuum
e3 = 80; %  e3--water
% >>>>>>>>>>>>>>>>>Other parameters<<<<<<<<<<<<<<<<<<
h = 6.626e-34; % Plack constant
kb = 1.38e-23; % Boltzman constant
avo = 6.022e23; % avogadro constant
T = 273.16 + 25; % Temperature
z = 1; % Valance
q = 1.602e-19; % electron charge
d0 = 12e-10; % surface-slipping plane distance
i=1;
list=[];
zetalist=[];
% >>>>>>>>>>>>>>>>>>>>>>>>> debye length <<<<<<<<<<<<<<<<<<<<
FAt = 2.99171*(10^-5);%((18.01596965)/(avo*1e-18));% acid A site density mol/m^2 ↙
where 0.75 is molecule/nm^2
FBt = 7.97788*(10^-5);%((48.04258574)/(avo*1e-18));% acid B site density mol/m^2 ↙
where 0.7  5 is molecule/nm^2
FDt = 6.64824*10^-8;%((0.015)/(avo*1e-18)); %base site 3.32115576*10^-8 0.015 ↙
molec/nm2, 3.191136*10^-4, 32 acceptor groups
FEt = 9.97235*(10^-6);%((((6.00532)/(avo*1e-18))));
ka = 10^(-5); % pka = -log(ka)carbox
kc = 10^(-10); %pka = -log(kc)phenol
kd = 10^(-10); %base pka  Base pka
ke = 10^(-8); %lactonic
syms zeta
psilist=[];
test=[];

%% >>>>>>>>>>>>>>>>>>>>>> surface potential <<<<<<<<<<<<<<<<<<<<<
while i<13;
    PH = i;
    i=i+1;
    dey = sqrt(e3*e0*kb*T/(q^2*z^2*(2*0.1*1e3)*avo)); % debye length
    inv = 1/dey;
    C1=q*avo;
    C2=(-q/(kb*T));
    C3=((e3*e0*inv*kb*T)/(2*pi*q));
    C4=(q/(2*kb*T));
    C5=2/inv;
    C6=(q/(4*kb*T));
    psi=((4*kb*T)/(z*q))*atanh(tanh((z*q*zeta)/(4*kb*T))*exp(inv*d0));
    FA=FAt/((((10^(-PH))*exp(C2*psi))/ka)+1);
    FB=FBt/((((10^(-PH))*exp(C2*psi))/kc)+1);
    FE=FEt/((((10^(-PH))*exp(C2*psi))/ke)+1);
    FD=FDt/(((((10^(-14))/(10^-PH))*exp(C2*psi))/kd)+1);
```

```
    sig1=C1*(-FA-FB-FE+FD);

    sig2=C3*(sinh(C4*psi)+(C5/(R2*10^-9))*tanh(C6*psi));
    sig3=sig1==sig2;

    ps=vpasolve(sig3,zeta);

    list(end+1)=(ps*1000);

end
phlist=[1,2,3,4,5,6,7,8,9,10,11,12];
plot(phlist,list),axis([0 13 -35 10]);
list
```

Figure 356: *Sample of glucose zeta potential mode MatLab code*

Appendix C: Zeta Potential Fits and Parameters

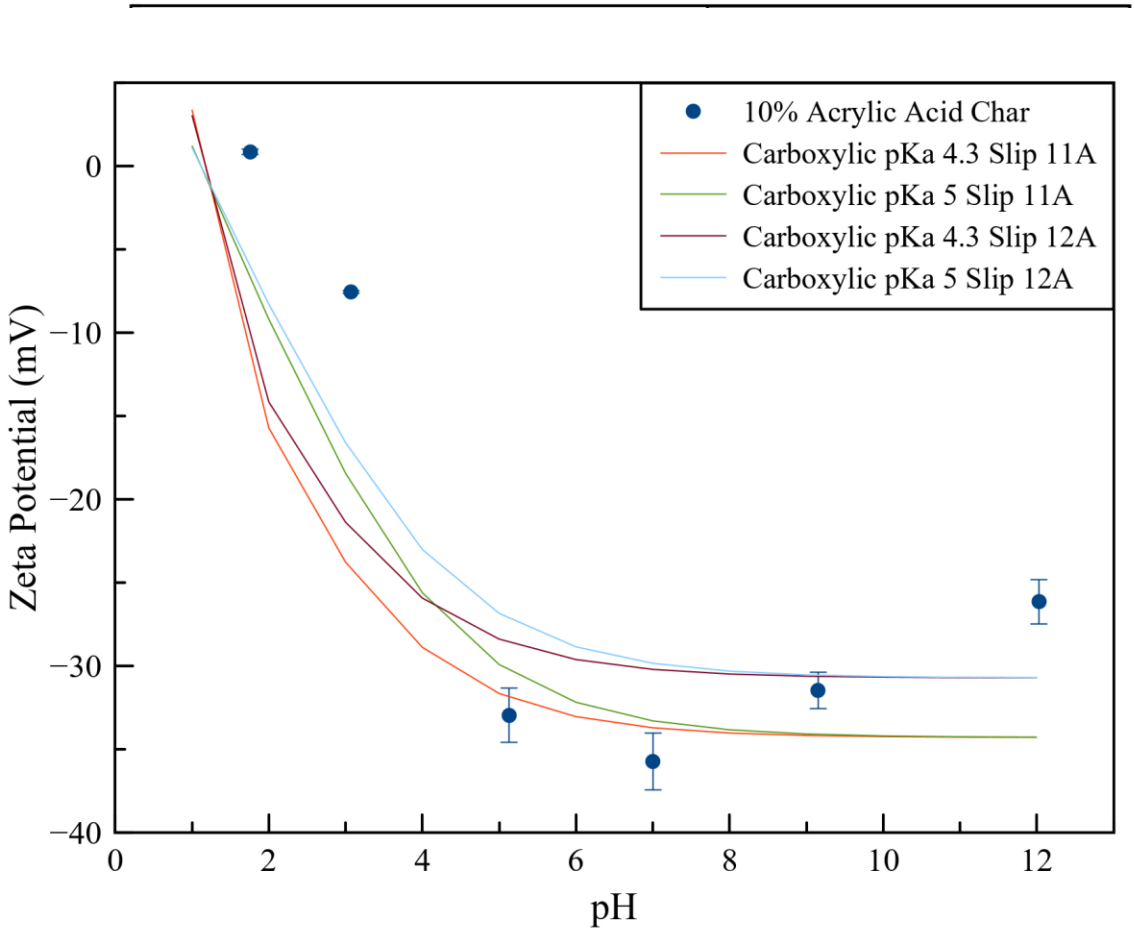

Figure 367: *5% Acrylic acid char zeta potential model curves; base pKa's used 14.5(carbox4.3) 15.15(carbox5)*

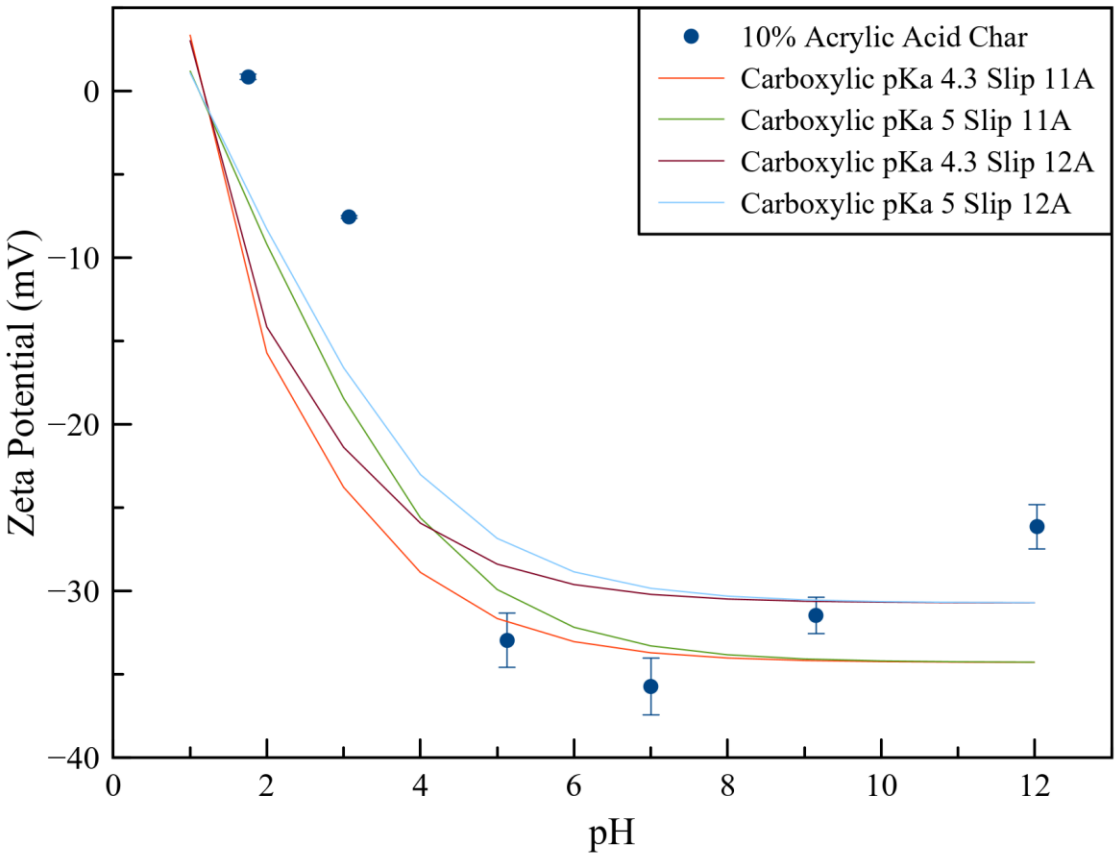

Figure 378: *10% Acrylic acid char zeta potential model curves; base pKa's used 15.46(carbox4.3) 16.2(carbox5)*

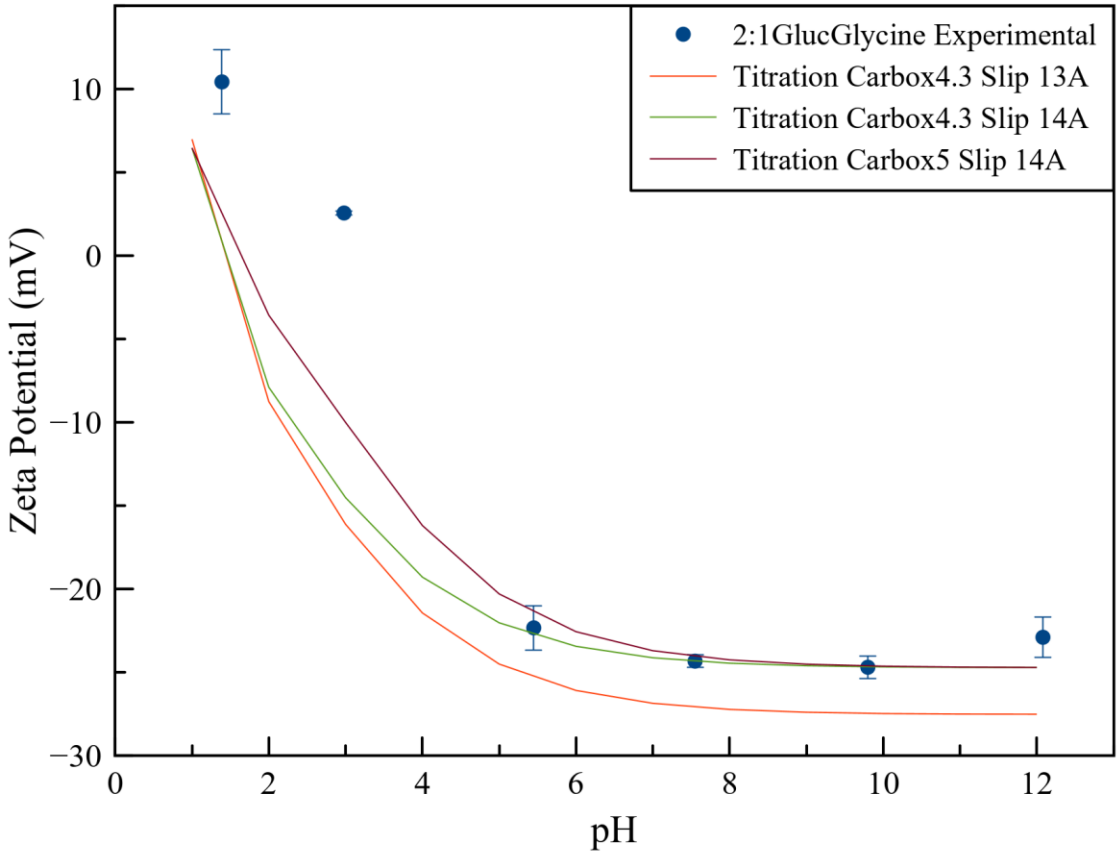

Figure 39: *Glycine char zeta potential model curves; base pKa's used 16.2952(carbox4.3) 16.5761(carbox5)*

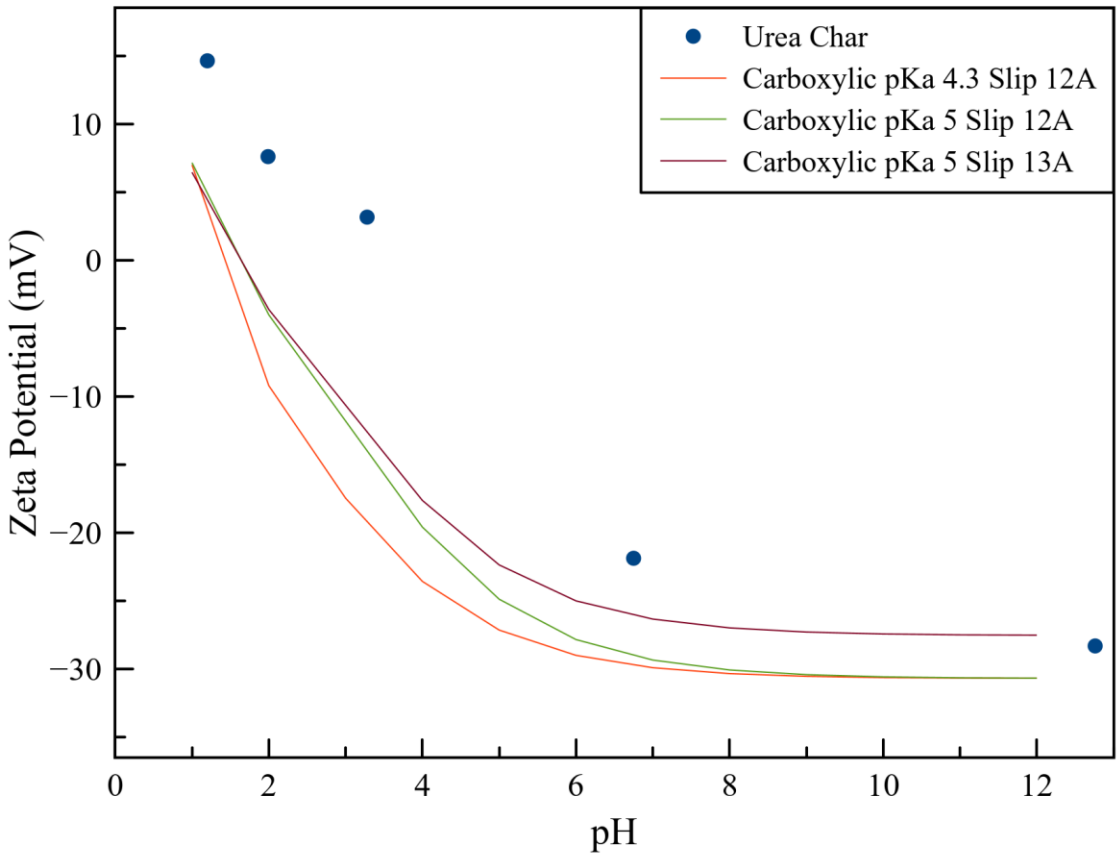

Figure 4038: *Urea char zeta potential model curves; base pKa's used 15.99(carbox4.3) 16.25(carbox5)*